

1 8 November 2017
2 Response to Reviewer #1
3
4 Reviewer#1 comments
5
6 Manuscript #: acp-2017-525
7 Manuscript title: Comparison of Global Observations and Trends of Total Precipitable
8 Water Derived from Microwave Radiometers and COSMIC Radio Occultation from 2006
9 to 2013

10
11 Brief Summary of the Manuscript:
12

13 This manuscript compares TPW estimates from the COSMIC radio occultation mission
14 against estimates from SSM/I, SSMIS, radiometers, and WindSat over clear sky and
15 cloudy conditions. The authors report a very good agreement between COSMIC and all
16 other TWP data sets and trends. They also claim that the estimated differences between
17 MW radiometers and COSMIC are mainly due to biases in the MW retrieval uncertainty
18 under cloudy and precipitating conditions. This analysis is in my opinion a novel
19 approach to establishing radio occultations as a new remote sensing climate instrument
20 by cross-comparing the COSMIC results with independent data sets. The manuscript is
21 very well written, coherent, and the results are presented nicely within the context of the
22 investigation. My recommendation for this manuscript is publication after minor
23 revisions, as described below.

24
25 ⇒ We thank the reviewer for his or her thoughtful comments and have incorporated
26 the suggested changes in the revised manuscript.
27

28 **Major Comments:**
29

30 1) Page 7; Line 147: What is the cut-off value of the liquid water column? Given that this
31 value
32 establishes an upper limit in the estimation of the TPW in the RSS products, could this
33 introduce a bias in the COSMIC vs RSS comparisons at high TPW values? I think this
34 must be explicitly discussed in the manuscript.
35

36 ⇒ As shown in the valid data range reported by RSS (see
37 <http://www.remss.com/missions/ssmi/>) the cut off values of the liquid water
38 column are from -0.05 to 2.45 mm (plus the offset value -0.05 mm).
39 ⇒ As demonstrated in Fig. 5d, the number of samples for RSS total cloud water
40 (liquid water column) for those MW-COSMIC pairs peaks at around 0.01 mm
41 (~2600) then decreases to fewer than 10 at 0.4 mm. The sample number for RSS
42 total cloud water value equal to or larger than the cut-off value (2.40 mm) is
43 therefore less than 10, which will not introduce any significant biases in the RSS
44 MW-COSMIC comparison.
45
46

47
48 2) Page 11; Line 236: The authors assume an 80% relative humidity below 0.1 km. What
49 is the sensitivity of the COSMIC TPW estimation the relative humidity assumption? How
50 does that affect the conclusions of this investigation?

51
52 ⇒ We added the following in Section 2.3: The COSMIC TPW estimates are not very
53 sensitive to the assumption of 80% relative humidity below 0.1 km (Step i above).
54 The assumption of 80%±10% (i.e., 90% and 70%) relative humidity below 0.1
55 km introduces an uncertainty of about ±0.03 mm uncertainty in the WV –
56 COSMIC comparisons for all conditions. As shown in Section 4, this uncertainty
57 is small compared to the observed differences between the RO and MW
58 estimates.

59
60 3) Lines 289–291, Lines 309–310, Lines 414–423: The authors conclude that the primary
61 source of the estimated biases between COSMIC and the rest of the data sets is the MW
62 retrieval uncertainty. Because the largest biases are found under cloudy precipitating
63 conditions, I think that the authors should also acknowledge that errors due to: a) cut-off
64 liquid water and b) the 80% RH assumption below 0.1 km, could also contribute to the
65 reported differences. Could there be a combined effect as well?

66
67 ⇒ As stated in our responses to major comment 1), the RSS pre-defined cut off
68 value for liquid water will not affect the conclusion from this study.
69 ⇒ As stated in our responses to major comment 2), the 80% RH assumption below
70 0.1 km does not affect the conclusions from this study.
71 ⇒ Since there is a very small number of RSS total cloud water values equal or larger
72 than the cut-off value (2.40 mm), there is no combined effect for these two
73 uncertainties that will affect the conclusion from this study.

74
75 4) Page 16; Line 357: It should read: “...with F15, F16, F17, and WindSat under...”

76
77 ⇒ Done

78
79
80 **Minor Comments:**

81
82 a) Line 57: Grammatically the sentence is fine, but the noun “increases” reads rather
83 awkward. Perhaps, consider replacing it with the word “enhancements”?

84
85 ⇒ “increases” is replaced by “enhancements”

86
87
88 b) Line 69: It should read: “reanalyses”.

89
90 ⇒ All of the “reanalysis” are replaced by “reanalyses”.

91
92 c) Line 92: Place a comma after the word “Recently”.

93
94 ⇒ Done
95
96 d) Line 116: Delete the word “and”
97
98 ⇒ Done
99
100 e) Line 161: It should read: “... (RR, in mm/hr), respectively, in 2007.”
101
102 ⇒ Done
103
104 f) Line 161: It should read: “temperature variations over the Intertropical Convergence
105 Zone (ITCZ) (Fig. 1b), which...”
106
107 ⇒ Done
108
109 g) Lines 181-182: It should read: “where P is the pressure in hPa, T is the temperature in
110 K, P_w is the water vapor pressure in hPa, W_{water} is the liquid water content in grams per
111 cubic meter (g m^{-3})...”
112
113 ⇒ Done
114
115 h) Line 208: Place a comma after the word “troposphere”.
116
117 ⇒ Done
118
119 i) Lines 216-218: I think that this statement is a bit bold. Perhaps, mention that the
120 “...retrieved water vapor profiles are weekly dependent on the first guess” and provide a
121 more appropriate reference that demonstrates that?
122
123 ⇒ In Line 226, “the retrieved water vapor profiles are insensitive to the first guess
124 water vapor profiles” is replaced with “the retrieved water vapor profiles are
125 weakly dependent on the first guess water vapor profiles (Neiman et al. 2008)”.
126 Neiman et al. (2008) is a good reference for this statement.
127
128 j) Line 244: Check “Wick2008”. Is it written properly?
129
130 ⇒ In Line 125 of the original manuscript (141-142 of revised manuscript), we
131 defined Wick et al.(2008) as “Wick2008” the first time the reference is given, so
132 “Wick2008” is ok.
133
134 k) Line 264: Spell out December.
135
136 ⇒ Done
137
138 l) Lines 264-266: Delete this sentence. It appears twice in Lines 259-260.

139
140 ⇒ Done
141
142 m) Line 268: It should read: “Figures 2a-d...”
143
144 ⇒ Done
145
146
147 n) Line 275: Explain briefly how the “rad-cal” beacon biases the F15 data.
148
149 ⇒ One sentence is added in Line 285, “On 14 August 2006, a radar calibration
150 beacon (RAD-CAL) was activated on F15. This radar interfered with the SSM/I,
151 primarily the 22V channel, which is a key channel for water vapor retrievals.
152 Although a correction method derived by *Hilburn and Wentz (2008)* and *Hilburn*
153 (2009) was applied, the 22 V channel is not being full corrected (Wentz, 2012).
154 As a result, there are still errors in the water vapor retrievals.”
155
156 ⇒ Two papers are added in to references:
157
158 Hilburn, K. A. and F. J. Wentz, 2008: Mitigating the Impact of RADCAL Beacon
159 Contamination on F15 SSM/I Ocean Retrievals. *Geophysical Research Letters*, 35.
160 L18806, doi:10.1029/2008GL034914.
161
162 Hilburn, K. A., 2009: Including Temperature Effects in the F15 RADCAL Correction.
163 *RSS Technical Report 051209*, Remote Sensing Systems, Santa Rosa, CA,
164 http://www.remss.com/papers/RSS_TR051209_RADCAL.pdf.
165
166
167 o) Line 300: It should read: “Figures 4a-d depict the...”
168
169 ⇒ Done
170
171
172 p) Line 318: It should read: “Figure 5b indicates that...”
173
174 ⇒ Done. And all “Fig.” replaced with “Figure” in the paper
175
176 q) Line 321: Delete “Fig. 5d”
177 ⇒ Done
178
179
180 r) Line 323: It should read: “Figure 5e shows that...”
181
182 ⇒ Done
183
184

185 s) Lines 338, 342: Spell out December.
186
187 ⇒ Done
188
189
190 t) Line 353: It should read: “Figure 8 depicts the...”
191
192 ⇒ Done
193
194
195 u) Line 366: It should read: “Figure 9 shows the...”
196
197 ⇒ Done
198
199
200 v) Line 382: It should read: “Figure 10 shows...”
201
202 ⇒ Done
203
204 w) Line 383: What about the F15 data?
205
206
207 ⇒ The reason we did not include F15 data in Figure 10 is mentioned in the last para
208 on page 17 of the revised manuscript: “The reason for larger standard deviations
209 of the MW minus RO differences for F15 (Tables 2 and 3 and Fig. 8a) is very
210 likely because the F15 data after August 2006 were corrupted by the “rad-cal”
211 beacon that was turned on at this time.” Also on this page “RSS does not
212 recommend using these measurements for studies of long-term change. Thus, we
213 consider the F15 data less reliable during the period of our study.”
214
215 x) Line 385: It should read: “...and west of Australia, south...”
216
217 ⇒ Done
218
219
220 y) Lines 399–400: It should read: “Because RO data have low sensitivity to clouds...”
221
222 ⇒ Done
223
224
225
226
227
228
229
230

231
232 9 November 2017
233 Response to Review #2
234
235
236 Anonymous Referee #2
237

238 This study compares passive microwave (MW) estimates of total precipitable water
239 (TPW) with radio occultation (RO) profiles of TPW that are closely matched together
240 in space and time. The comparison is broken into four parts: clear sky, cloudy sky,
241 cloudy sky with no precipitation, and cloudy sky with precipitation. The bias is smallest
242 in clear sky and is largest within precipitating conditions. The bias is shown to be
243 a small function of surface temperature, surface wind speed, etc., but these effects
244 have little consequence on the interpretation of biases and trends, which lends further
245 confidence to the results of this work. The trends in TPW are statistically significant
246 and are larger than previously reported. The trends are uniformly largest within cloudy
247 non-precipitating skies, and can be slightly negative in clear sky for a few of the MW
248 radiometers.
249

250 This is a very straightforward and useful study that is well written and flows logically.
251 I only have a few minor comments and suggestions before this paper is accepted for
252 publication.
253

254 ⇒ We thank this reviewer for his or her thoughtful comments, and we have
255 incorporated them into the revised manuscript.
256

257 1. Abstract and elsewhere: non-precipitating and precipitating conditions instead of
258 non-precipitation and precipitation conditions? I'm not an expert in grammar but the
259 latter
260 reads a little odd.
261

262 ⇒ To be consistent, we use precipitating and non-precipitating throughout in the revised
263 paper.
264

265 2. Lines 52-54: is the global water vapor feedback still one of the largest uncertainties?
266 We seem to know that the water vapor+lapse rate feedback has less spread in climate
267 models than cloud feedbacks (see Soden et al., 2008, J. Climate, Figure 7, and other
268 references). The role of water vapor and its regional variability, such as shown in Figure
269 10 in the manuscript, is probably the more uncertain quantity rather than global trends
270 as shown in Figure 9. To summarize, it might be better to emphasize the role of water
271 vapor in controlling cloud processes, and observing long term trends in water vapor is
272 part of that understanding.
273

274 ⇒ We have revised the introductory paragraph to incorporate these comments. In
275 addition, we added the following paper to the references:
276

277 Held, I. M., and B. J. Soden, 2000: Water vapor feedback and global warming, *Annu.*
 278 *Rev. Energy Environ.*, 25, 441–475, doi:10.1146/annurev.energy.25.1.441.
 279

280 Soden, B.J. and I.M. Held, 2006: Assessment of climate feedbacks in coupled ocean-
 281 atmosphere models. *J. Climate*, 19, 3354-3360.
 282

283 Wentz, F.J., Lucrezia Riccardulli, K. Hilburn, and C. Mears, 2007: How much more rain
 284 will global warming bring? *Science*, 317, 233-235.
 285

286 3. Line 66: land and ocean
 287 ⇒ We think it is more proper to use “lands and oceans”.
 288 ⇒ We changed this to “land areas and oceans.”
 289

290 4. Line 68: ocean
 291
 292 ⇒ We still use “oceans” since this means all “oceans”.
 293

294 5. Line 195: IWC can be even a bit higher than that in convective towers, see D. Leroy
 295 et
 296 al., 2017, *J. Atmos. Ocean Tech.* that summarizes the HAIC/HIWC field campaign
 297
 298 ⇒ We added “Heymsfield et al., (2002) reported high ice water content values
 299 ranging from 0.1 – 0.5 gm⁻³ in tropical cirrus and stratiform precipitating clouds,
 300 although it may rarely reach as high as 1.5 gm⁻³ in deep tropical convective clouds
 301 (Leroy et al., 2017).” We also added two references:
 302

303 Leroy, D., Fontaine, E., Schwarzenboeck, A., Strapp, J. W., Korolev, A., McFarquhar,
 304 G., Dupuy, R., Gourbeyre, C., Lilie, L., Protat, A., Delanoë, J., Dezitter, F., and Grandin,
 305 A., 2017: Ice crystal sizes in high ice water content clouds. Part 2: Statistics of mass
 306 diameter percentiles in tropical convection observed during the HAIC/HIWC project, *J.*
 307 *Atmos. Oceanic Technol.*, doi: 10.1175/JTECH-D-15-0246.1.
 308

309 Heymsfield, A. J., A. Bansemer, P. R. Field, S. L. Durden, J. L. Stith, J. E. Dye, W. Hall,
 310 and C. A. Grainger, 2002: Observations and parameterizations of particle size
 311 distributions in deep
 312 tropical cirrus and stratiform precipitating clouds: Results from in situ observations in
 313 TRMM field campaigns. *J. Atmos. Sci.*, 59, 3457–3491, doi:10.1175/1520-
 314 0469(2002)059, 3457.
 315

316 6. Lines 233-234: what is the percent frequency of COSMIC water vapor profiles
 317 that
 318 sample below 0.1 km?
 319
 320 ⇒ We added “About 70% to 90% of COSMIC profiles reach to within 1 km of the
 321 surface (Anthes et al, 2008). Usually more than 30% of COSMIC water vapor
 322 profiles reach below 0.1 km in the mid-latitudes and higher latitudes, and a little bit
 323 less than 10% in the tropical regions.”

324
325 7. Lines 246-249: the larger spatial variance of water vapor in the tropics compared to
326 the
327 extratropics should be reflected in the higher standard deviations, and their increases
328 sensitivity to collocation distance. Have the authors explored these differences? Would
329 also be helpful to cite a paper or two on the spatial variance of water vapor.
330
331 ⇒ Yes, the larger spatial variance of water vapor in the tropics compared to the
332 extratropics (see Fig. 1a) should be reflected in the higher standard deviations.
333 However, because RSS TPW retrieval errors could also be larger over stronger
334 convective regions under cloud and precipitating conditions (see section 4 and
335 Figs. 5 and 6), it is hard to distinguish the tropical vs. sub-tropical effect from
336 retrieval uncertainty effects.
337 ⇒ We added two sentences in the end of the paragraph “Note that, although not
338 shown, the mean biases and standard deviations of the mean biases are slightly
339 larger over the tropics than those over mid-latitudes. This could be because of the
340 combined effect of the larger spatial TPW variation in the tropics than those in the
341 mid-latitudes (see Fig. 1a, and Neiman et al., 2008; Teng et al., 2013; Mears et al.,
342 2015) and the fact that the MW TPW retrieval uncertainty is also larger over
343 stronger convection regions. More results are detailed in Section 4.”
344
345 8. Line 250: a little bit of extra clarification on the matchups is warranted. Does one
346 really get 20-60 MW pixels near a RO observation within a 1-hour period? This seems
347 excessive. Is this at 0.25 degrees resolution or a larger distance? Are the matchups for
348 the entire length of the 200 km RO or with respect to the tangent point at a particular
349 reference altitude?
350
351 ⇒ As mentioned in Section 2.3, “Pairs of MW and RO TPW estimates collocated
352 within 50 km and one hour are collected.” Over tropical regions, 0.25 degrees is
353 about 25 km. So one RO observation can match with about 16 (4x4) 0.25x0.25
354 MW grids. In higher latitudes, a 0.25 degree resolution is less than 25 km. So
355 within 50 km radius (100 km diameter), one RO observation can match from 16
356 (4x4) to 49 (7x7 in very high latitude) MW 0.25x0.25 grids. Although it is not
357 mentioned in the text, there are about 1 to 2 MW pixels binned into each
358 0.25x0.25 grid. Therefore, in the text, we mention that we will have about 20-60
359 MW pixels near a RO observation.
360 ⇒ Again, the matchup is within 50 km at the location of RO tangent point at 4-5 km
361 altitude. We added the statement “The location of RO observation is defined by
362 the RO tangent point at 4-5 km altitude.”
363
364 9. Line 268: Figures 3a-c (only three panels)
365
366 ⇒ It should refer to Fig. 2 not Fig. 3, and is revised to “Figures 2a-d”
367
368 10. Line 298: under different
369

370 ⇒ Done
371
372 11. Line 310: a small but significant degree seems a little bit contradictory, maybe there
373 is
374 a better way to state this
375
376 ⇒ “a small but significant degree” is replaced by “which in turn affect the MW TPW
377 retrievals.
378
379 12. Line 314: droplets
380
381 ⇒ Done
382
383
384 13. Line 385: Australian, and also South America
385
386 ⇒ Done
387
388 14. Line 412: reliable references
389
390 ⇒ “reliable reference data” is used.
391
392
393 15. Lines 432-440: can the authors say anything about the magnitudes of these trends
394 and
395 whether they are consistent with the constant RH hypothesis of Earth’s atmosphere?
396
397 ⇒ This is a good question, but also one that is difficult to answer from our results. We
398 added the following to the end of the Discussion section:
399
400 Other studies have suggested that this positive feedback results in a nearly constant
401 global mean relative humidity (Soden and Held, 2006; Sherwood et al., 2010). However,
402 it is difficult to directly relate our estimated TPW trends to constant RH hypothesis of
403 Earth’s atmosphere under global warming. The global mean surface temperature has been
404 rising at about the rate of 0.2 K/decade in the past twenty years. A 0.2K increase in
405 temperature would produce about a 1.4% increase in saturation water vapor pressure based
406 on the Clausius-Clapeyron equation. To maintain a constant RH for this temperature
407 increase, the actual water vapor pressure (and specific humidity) would also have to
408 increase by 1.4%. In this study, we observe an increase of TPW in our dataset of about 1.78
409 mm/decade which is 6.9 percent increase per decade in TPW. Our dataset is dominated
410 mainly by cloudy samples over middle latitudes (40°N-60°N and 40°-65°S). Thus, from
411 these numbers alone we would expect an increase in mean RH under cloudy conditions by
412 more than 6%, which is unlikely and well outside the range of changes in relative humidity
413 in models (e.g. Figure 2 in Sherwood et al., 2010). However, the changes in the global
414 mean RH are not related in such a simple fashion to changes in the global mean temperature
415 and precipitable water. For example, Figure 10 depicts that there are very large differences

416 in the spatial distribution of TPW changes, which shows regional variations of +/- 4
417 mm/decade. Thus, some regions are drying and others are moistening. The variations in
418 global mean surface temperature are also large, but very different from those of TPW, with
419 the polar regions and continents warming up much faster than the atmosphere over the
420 oceans. In cold polar regions, an increase in temperature will result in a smaller increase in
421 saturation vapor pressure than the same increase in temperature in the tropics. The global
422 evaporation and precipitation patterns also vary greatly, as water vapor transport is
423 important in the global water vapor balance. All of this, as discussed by Held and Soden
424 (2000), Soden and Held (2006), and Sherwood et al. (2010) means that the relationships
425 between global mean temperature increase, TPW changes, and the resulting change in
426 global mean RH are not simple.

427
428

429 16. Line 494: author list for reference is incomplete

430

431 All of the authors are added in the reference. The new reference is "Fetzer, E. J., W.G.
432 Read, D. Waliser, B. H. Kahn, B. Tian, H. Vömel, F. W. Irion, H. Su, A. Eldering,
433 M. T. Juarez, J. Jiang, and V. Dang, 2008: Comparison of upper tropospheric water
434 vapor observations from the Microwave Limb Sounder and Atmospheric Infrared
435 Sounder. *J. Geophys. Res.*, 113/D22, D22110."

436

437

438

439

440

441

442

443

444

445

446

447

448

449

450

451

452

453

454

455

456

457

458

459

460

461

462 9 November 2017
463 Revised draft with changes shown (tracking on)
464

465

466 **Comparison of Global Observations and Trends of Total Precipitable Water Derived**
467 **from Microwave Radiometers and COSMIC Radio Occultation from 2006 to 2013**

468

469

470 Shu-peng Ho¹, Liang Peng¹, Carl Mears², Richard A. Anthes¹

471 ¹ University Corporation for Atmospheric Research, P.O. Box 3000, Boulder, CO. 80307-

472 3000

473 ² Remote Sensing Systems, Santa Rosa, California, USA,

474 Corresponding author address: Dr. Shu-Peng Ho, COSMIC Project Office, University

475 Corporation for Atmospheric Research, P. O. Box 3000, Boulder CO. 80307-3000

476 E-mail: spho@ucar.edu

477

478

479 Manuscript for Atmospheric Chemistry and Physics

480

481 9 November 2017

482

483 Shu-Peng Ho, COSMIC Project Office, Univ. Corp. for Atmospheric Research, P. O.

484 Box 3000, Boulder CO. 80307-3000, USA (spho@ucar.edu)

485

486

487

488

Deleted: 2

490 **Abstract**

491 We compare atmospheric total precipitable water (TPW) derived from SSM/I (Special
492 Sensor Microwave Imager) and SSMIS (Special Sensor Microwave Imager Sounder)
493 radiometers and WindSat to collocated TPW estimates derived from COSMIC
494 (Constellation System for Meteorology, Ionosphere and Climate) radio occultation (RO)
495 under clear and cloudy conditions over the oceans from June 2006 to December 2013.
496 Results show that the mean microwave (MW) radiometer - COSMIC TPW differences
497 range from 0.06-0.18 mm for clear skies, 0.79-0.96 mm for cloudy skies, 0.46-0.49 mm for
498 cloudy but non-precipitating conditions, and 1.64-1.88 mm for precipitating conditions.
499 Because RO measurements are not significantly affected by clouds and precipitation, the
500 biases mainly result from MW retrieval uncertainties under cloudy and precipitating
501 conditions. All COSMIC and MW radiometers detect a positive TPW trend over these eight
502 years. The trend using all COSMIC observations collocated with MW pixels for this data
503 set is 1.79 mm/decade, with a 95% confidence interval of (0.96, 2.63), which is in close
504 agreement with the trend estimated by the collocated MW observations (1.78 mm/decade
505 with a 95% confidence interval of 0.94, 2.62). The sample of MW and RO pairs used in
506 this study is highly biased toward middle latitudes (40°-60°N and 40°-65°S), and so these
507 trends are not representative of global average trends. However, they are representative of
508 the latitudes of extratropical storm tracks and the trend values are approximately four to
509 six times the global average trends, which are approximately 0.3 mm/decade. In addition,
510 the close agreement of these two trends from independent observations, which represent
511 an increase in TPW in our data set of about 6.9%, are a strong indication of the positive
512 water vapor-temperature feedback in a warming planet in regions where precipitation from

Deleted: on

Deleted: on

Deleted: all

Deleted: year

Deleted: are larger than previous estimates and

§18 extratropical storms is already large.

519

520

521

522

523

524

525

526

527

528

529

530

531

532

533

534

535

536

537

538

539

540

541 **1. Introduction**

542 Clouds are important regulators for Earth's radiation and hydrological balances.

543 Water vapor is a primary variable that affects cloud radiative effects and hydrological

544 feedbacks. In addition, the three-dimensional distribution of water vapor is a key factor for

545 cloud formation and distribution (Soden et al., 2002), Held and Soden (2000) and Soden

546 and Held (2006) illustrated that water vapor amounts will increase in response to global

547 warming. Climate models predict that the column-integrated amount of water vapor, or

548 total precipitable water, will increase by ~7% per 1 K increase in surface temperature

549 (Wentz and Schabel, 2000; Trenberth et al., 2005; Wentz et al., 2007). Therefore, accurate

550 observations of long-term water vapor under both clear and cloudy skies are important for

551 understanding the role of water vapor on climate as well as cloud formation and

552 distribution, which is still one of the largest uncertainties in understanding climate change

553 mechanisms (IPCC 2013). Trends in global and regional vertically integrated total

554 atmospheric water vapor, or Total Precipitable Water (TPW), are important indicators of

555 climate warming because of the strong positive feedback between temperature and water

556 vapor enhancements. Accurate observations of TPW are therefore important in identifying

557 climate change and in verifying climate models, which estimate a wide range of TPW

558 trends (Roman et al. 2014).

559 The TPW depends on temperature (Trenberth and Guillemot, 1998; Trenberth et

560 al., 2005). Global TPW can be derived from satellite visible, infrared, and microwave

561 sensors (i.e., Wentz and Spencer, 1998; Fetzer et al. 2006; John and Soden, 2007; Fetzer

562 et al. 2008; Noël et al. 2004). However, no single remote sensing technique is capable of

563 completely fulfilling the needs for climate studies in terms of spatial and temporal coverage

Deleted: , which is modulated by convection and the hydrological cycle

Deleted: A

Deleted: increases

568 and accuracy. For example, while water vapor retrievals from visible and infrared satellite
569 sensors are limited to clear skies over both land [areas](#) and oceans, passive microwave (MW)
570 imagers on satellites can provide all sky water vapor products, but only over oceans. These
571 water vapor products are mainly verified by comparing to either reanalyses, radiosonde
572 measurements, or other satellite data (i.e., Soden, and Lanzante, 1996; Sohn and Smith,
573 2003; Noël et al. 2004; Palm et al. 2008; Sohn and Bennartz, 2008; Wick et al. 2008
574 [\(hereafter Wick2008\)](#); Milz et al. 2009; Prasad and Singh, 2009; Pougatchev et al. 2009;
575 Knuteson et al., 2010; Larar et al. 2010; Wang et al. 2010; Ho et al. 2010a, b). Results from
576 these validation studies show that the quality of water vapor data from different satellite
577 sensors varies under different atmospheric conditions. The change of reanalysis systems
578 and inconsistent calibration among data may also cause uncertainty in long-term stability
579 of water vapor estimates. In addition, it is well known that radiosonde sensor characteristics
580 can be affected by the changing environment (Luers and Eskridge, 1998; Wang and Zhang,
581 2008). Ho et al. (2010b) demonstrated that the quality of radiosonde humidity
582 measurements varies with sensor types, adding extra difficulties in making a consistent
583 validation of long term water vapor products.

584 MW imagers are among the very few satellite instruments that are able to provide
585 long-term (close to 30 years) all-weather time series of water vapor measurements using
586 similar sensors and retrieval techniques (Wentz, 2015). The measured radiances at 19.35,
587 22.235, and 37.0 GHz from SSMIS and 18.7, 23.8, and 37.0 GHz from WindSat are used
588 to derive TPW, total cloud water (TCW), wind speed, and rainfall rates over oceans (Wentz
589 and Spencer, 1998). These four variables are retrieved by varying their values until the
590 brightness temperatures calculated using a forward model match satellite-observed

Deleted: s

Deleted: i

593 brightness temperatures. Because MW radiation is significantly affected (absorbed or
594 scattered) by heavy rain, these four variables are only retrieved under conditions of no or
595 light-to-moderate rain (Schlüssel and Emery, 1990; Elsaesser and Kummerow, 2008;
596 Wentz and Spencer, 1998).

597 Recently, version 7.0 daily ocean products mapped to a 0.25° grid derived from
598 multiple MW radiometers were released by Remote Sensing System (RSS) (Wentz, 2013).
599 Many validation studies have been performed by RSS by comparing the MW TPW
600 retrievals with those from ground-based Global Positioning System (gb-GPS) stations
601 (Mears et al, 2015; Wentz, 2015). Because the gb-GPS stations are nearly always located
602 on land, these validation studies use stations located on small and isolated islands (Mears
603 et al., 2015). RSS results for TPW collocated with those derived from gb-GPS over these
604 island stations show that their mean differences vary from station to station, and can be as
605 large as 2 mm. The mean difference also varies with surface wind speed, varying from 1
606 mm at low wind speeds to -1 mm at high wind (20 m/s) speeds. The difference is near zero
607 for the most common wind speeds (6 to 12 m/s). Because the uncertainty of the input
608 parameters and change of antenna for each GPS receiver (Bock et al., 2013), the mean
609 TPW(RSS) – TPW (gb-GPS) can vary from -1.5 mm to 1.5 mm for a single MW radiometer
610 (see Figure 4 in Mears et al., 2015). Wentz (2015) compared 17 years of Tropical Rainfall
611 Measuring Mission (TRMM) Microwave Imager (TMI) TPW collocated with gb-GPS
612 TPW over the region from 45°N to 45° S. The mean TMI- gb-GPS TPW bias was estimated
613 to be 0.45 mm with a standard deviation (σ) of 2.01 mm.

614 Unlike passive MW radiometers and infrared sensors, radio occultation (RO) is an
615 active remote sensing technique. RO can provide all-weather, high vertical resolution (from

616 ~100 m near the surface to ~1.5 km at 40 km) refractivity profiles (Anthes, 2011). The
617 basis of the RO measurement is a timing measured against reference clocks on the ground,
618 which are timed and calibrated by the atomic clocks at the National Institutes for Standards
619 and Technology (NIST). With a GPS receiver onboard the LEO (Low-Earth Orbiting)
620 satellite, this technique is able to detect the bending of radio signals emitted by GPS
621 satellites, traversing the atmosphere. With the information about the relative motion of the
622 GPS and LEO satellites, the bending angle profile of the radio waves can be used to derive
623 all-weather refractivity, pressure, temperature, and water vapor profiles in the neutral
624 atmosphere (Anthes et al., 2008).

Deleted: c
Deleted: s

625 Launched in June 2006, COSMIC (Constellation Observing System for
626 Meteorology, Ionosphere, and Climate) RO data have been used to study atmospheric
627 temperature and refractivity trends in the lower stratosphere (Ho et al., 2009a, b, and 2012),
628 and modes of variability above, within, and below clouds (Biondi et al., 2012, 2013; Teng
629 et al., 2013; Scherllin-Pirscher et al., 2012; Zeng et al., 2012; Mears et al., 2012). Wick2008
630 demonstrated the feasibility of using COSMIC-derived TPW to validate SSM/I TPW
631 products over the east Pacific Ocean using one month of data. Many studies have
632 demonstrated the usefulness of RO derived water vapor to detect climate signals of El
633 Niño–Southern Oscillation (ENSO; Teng et al., 2013; Scherllin-Pirscher et al, 2012; Huang
634 et al., 2013), Madden-Julian Oscillation (MJO; Zeng et al., 2012), and improving moisture
635 analysis of atmospheric rivers (Neiman et al., 2008; Ma et al. 2011).

Deleted: and

Deleted: Wick et al., (2008) (
Deleted: hereafter)

636 The objective of this study is to use COSMIC RO TPW to characterize the global
637 TPW values and trends derived from multiple MW radiometers over oceans, including
638 under cloudy and precipitating skies. COSMIC TPW from June 2006 to December 2013

644 are compared to ~~co-~~located TPW derived from MW radiometers over the same time period.

Deleted: the

645 Because RO data are not strongly sensitive to clouds and precipitation, COSMIC TPW
646 estimates can be used to identify possible MW TPW biases under different meteorological
647 conditions. We describe datasets and analysis method used in the comparisons in Section
648 2. The comparison results under clear skies and cloudy skies are summarized in Sections 3
649 and 4, respectively. The time series analysis is in Section 5. We conclude this study in
650 Section 6.

651

652 **2. RSS Version 7.0 Data and COSMIC TPW Data and Comparison Method**

653 **2.1 RSS Version 7.0 Data Ocean Products**

654 The RSS version 7.0 ocean products are available for SSM/I, SSMIS, AMSR-E,
655 WindSat, and TMI. The inversion algorithm is mainly based on Wentz and Spencer,
656 (1998), where above a cutoff in the liquid water column (2.45 mm), water vapor is no
657 longer retrieved. The various radiometers from the different satellites have been precisely
658 inter-calibrated at the radiance level by analyzing the measurements made by pairs of
659 satellites operating at the same time. This was done for the explicit purpose of producing
660 versions of the datasets that can be used to study decadal-scale changes in TPW, wind,
661 clouds, and precipitation, so special attention was focused on inter-annual variability in
662 instrument calibration. The calibration procedures and physical inversion algorithm used
663 to simultaneously retrieve TPW, surface wind speed (and thereby surface wind stress and
664 surface roughness) and the total liquid water content are summarized in Wentz (2013) and
665 Wentz (1997), respectively. This allows the algorithm to minimize the effect of wind speed,
666 clouds, and rain on the TPW measurement.

Deleted: ed

669 The RSS version 7.0 daily data are available on a 0.25° latitude x 0.25° longitude
 670 grid for daytime and nighttime (i.e., 1440x720x2 daily per day). Figures 1a-d shows the
 671 RSS V7.0 monthly mean F16 SSMIS TPW (in mm), surface skin temperature (in K), liquid
 672 water path (LWP, in mm), and rain rate (RR, in mm/h), respectively, in 2007. Figure 1
 673 shows that the variation and distribution of TPW over oceans (Figure 1a) is, in general,
 674 closely linked to surface skin temperature variations over the Intertropical Convergence
 675 Zone (ITCZ) (Figure 1b), which is modulated by clouds and the hydrological cycle (Soden
 676 et al., 2002). The distribution of monthly TPW is consistent with that of cloud water, where
 677 highest TPW values (and LWP and RR) occur in persistent cloudy and strong convective
 678 regions over the tropical west Pacific Ocean near Indonesia.

679 Because COSMIC reprocessed TPW data are only available from June 2006 to
 680 December 2013 (i.e., COSMIC2013), the SSM/I F15, SSMIS F16, SSMIS F17, together
 681 with WindSat, RSS Version 7.01 ocean products covering the same time period are used in
 682 this study. Table 1 summarizes the starting date and end date for RSS SSM/I F15, SSMIS
 683 F16, SSMIS F17, and WindSat data. The all sky daily RSS ocean products for F15, F16,
 684 F17, and WindSat are downloaded from <http://www.remss.com/missions/ssmi>.

685
 686 **2.2 COSMIC TPW Products**

687 The atmospheric refractivity N is a function of pressure P, temperature T, water
 688 vapor pressure P_w , and water content W through the following relationship (Kursinski
 689 1997; Zou et al. 2012):

690
 691
$$N = 77.6 \frac{P}{T} + 3.73 \times 10^5 \frac{P_w}{T^2} + 1.4W_{\text{water}} + 0.61W_{\text{ice}} \quad (1)$$

Deleted: r
 Deleted: our
 Deleted: .
 Deleted: .

Deleted: (Fig. 1b),

Deleted: ose
 Deleted: vapor distribution patterns

Deleted: AT

Deleted: AT

Deleted: the

702

703 where P is the pressure in hPa, T is the temperature in K, P_w is the water vapor pressure in
704 hPa, W_{water} is the liquid water content in grams per cubic meter (gm^{-3}), and W_{ice} is the
705 ice water content in gm^{-3} . The last two terms generally contribute less than 1% to the
706 refractivity and may be ignored (Zou et al., 2012). However, they can be significant for
707 some applications under conditions of high cloud liquid or ice water content, as shown by
708 Lin et al. 2010; Yang and Zou 2012; Zou et al. 2012. We will neglect these terms in this
709 study, but because we are looking at small differences between MW and RO TPW in
710 cloudy and precipitating conditions in this paper, we estimate the possible contribution of
711 these terms to RO TPW and the consequences of neglecting them here. Since both of these
712 terms increase N, neglecting them in an atmosphere in which they are present will produce
713 a small positive bias in water vapor pressure P_w and therefore total precipitable water when
714 integrated throughout the entire depth of the atmosphere.

715 Typical value of cloud LWC range from $\sim 0.2 \text{ gm}^{-3}$ in stratiform clouds (Thompson,
716 2007) to 1 gm^{-3} in convective clouds (Thompson, 2007; Cober et al. 2001). Extreme values
717 may reach $\sim 2 \text{ gm}^{-3}$ in deep tropical convective clouds (i.e., cumulonimbus). Ice water
718 content values are smaller, typically $0.01 - 0.03 \text{ gm}^{-3}$ (Thompson, 2007). Heymsfield et al.,
719 (2002) reported high ice water content values ranging from $0.1 - 0.5 \text{ gm}^{-3}$ in tropical cirrus
720 and stratiform precipitating clouds, although it may rarely reach as high as 1.5 gm^{-3} in deep
721 tropical convective clouds (Leroy et al., 2017).

722 For extremely high values of W_{water} and W_{ice} of 2.0 and 0.5 gm^{-3} , the contributions
723 to N are 2.8 and 0.3 respectively. The values of N in the atmosphere decrease exponentially
724 upward, from ~ 300 near the surface to ~ 150 at $P=500$ hPa. Using the above extreme values

Deleted: 6

Deleted: (Thompson, 2007). .

727 at 500 hPa, W_{water} may contribute from up to 1.6% of N and W_{ice} up to 0.2%. Thus we may
728 assume that in most cases the error in N due to neglecting these terms will be less than 1%.
729 The effect on TPW will be even less, since clouds do not generally extend through the full
730 depth of the atmosphere. Finally, the ~200 km horizontal averaging scale of the RO
731 observation footprint makes it unlikely that such extremely high values of water and ice
732 content will be present over this scale. We conclude that the small positive bias in RO TPW
733 introduced by neglecting the liquid and water terms in (1) will be less than 1%.

734 To resolve the ambiguity of COSMIC refractivity associated with both temperature
735 and water vapor in the lower troposphere, a 1D-var algorithm ([http://cosmic-
737 io.cosmic.ucar.edu/cdaac/doc/documents/1dvar.pdf](http://cosmic-
736 io.cosmic.ucar.edu/cdaac/doc/documents/1dvar.pdf)) is used to derive optimal temperature
738 and water vapor profiles while temperatures and water vapor profiles from the ERA-
739 Interim reanalysis are used as a priori estimates (Neiman et al. 2008; Zeng et al. 2012).

739 Note that because RO refractivity is very sensitive to water vapor variations in the
740 troposphere (Ho et al. 2007), and is less sensitive to temperature errors, RO-derived water
741 vapor product is of high accuracy (Ho et al. 2010 a, b). It is estimated that 1K of
742 temperature error will introduce less than 0.25 g/kg of water vapor bias in the troposphere
743 in the 1D-var retrievals. Although the first guess temperature and moisture are needed for
744 the 1D-Var algorithm, the retrieved water vapor profiles are weakly dependent on the first
745 guess water vapor profiles (Neiman et al. 2008).

746 The horizontal footprint of a COSMIC observation is about 200 km in the lower
747 troposphere and its vertical resolution is about 100 m near the surface and 1.5 km at 40 km.

748 The COSMIC post-processed water vapor profiles version 2010_2640 collected from
749 COSMIC Data Analysis and Archive Center (CDAAC)

Deleted: insensitive to

Deleted: 3

752 (<http://cosmic.cosmic.ucar.edu/cdaac/index.html>) are used to construct the COSMIC
753 TPW data. To further validate the accuracy of COSMIC-derived water vapor, we have
754 compared COSMIC TPW with those derived from ground-based GPS (i.e., International
755 Global Navigation Satellite Systems–IGS, Wang et al. 2007) which are assumed to be
756 independent of location. Only those COSMIC profiles whose lowest penetration heights
757 are within 200 meters of the height of ground-based GPS stations are included. Results
758 showed that the mean global difference between IGS and COSMIC TPW is about -0.2 mm
759 with a standard deviation of 2.7 mm (Ho et al., 2010a). Similar comparisons were found
760 by Teng et al. (2013) and Huang et al. (2013).

761

762 2.3 Preparation of COSMIC TPW data for Comparison

763 In this study, only those COSMIC water vapor profiles penetrating lower than 0.1
764 km are integrated to compute TPW. ~~Approximately, 70% to 90% of COSMIC profiles~~
765 ~~reach to within 1 km of the surface (Anthes et al., 2008). Usually more than 30% of~~
766 ~~COSMIC water vapor profiles reach below 0.1 km in the mid-latitudes and higher latitudes,~~
767 ~~and a little bit less than 10% in the tropical regions.~~ To compensate for the water vapor
768 amount below the penetration height, we follow the following procedure:

- 769 i) we assume the relative humidity below the penetration height is equal to 80%. This is
770 a good assumption especially over oceans near the sea surface (Mears et al., 2015);
771 ii) the temperatures below the penetration height are taken from the ERA-interim
772 reanalysis;
773 iii) we compute the water vapor mixing ratio below the penetration heights;

Deleted: As stated in Anthes et al., (2008),

Deleted:

Deleted: that

Deleted: a

Deleted: bout

Deleted: we will have

Deleted: are sampled

781 iv) we integrate the TPW using COSMIC water vapor profiles above the penetration
782 heights with those water vapor profile below the penetration heights.

783 The COSMIC TPW estimates are not very sensitive to the assumption of 80% relative
784 humidity below 0.1 km (Step i above). The assumption of 80% +/-10% (i.e., 90% and 70%)
785 relative humidity below 0.1 km introduces an uncertainty of about +/- 0.03 mm in the WV
786 - COSMIC comparisons for all conditions. As shown in Section 4, this uncertainty is small
787 compared to the observed differences between the RO and MW estimates.

788 Pairs of MW and RO TPW estimates collocated within 50 km and one hour are
789 collected. The location of RO observation is defined by the RO tangent point at 4-5 km
790 altitude. Wick2008 used MW-RO pairs within 25 km and one hour in time. To evaluate
791 the effect of the spatial difference on the TPW difference, we also computed TPW
792 differences for MW-RO pairs within 75 km, 100 km, and 150 km, and 200 km. We found
793 the larger spatial difference increases the mean TPW biases slightly to +/- 0.25 mm and the
794 standard deviations to +/- 1.91 mm, which is likely because of the high spatial variability
795 of water vapor. Note that, although not shown, the mean biases and standard deviations of
796 the mean biases are slightly larger over the tropics than over mid-latitudes. This could be
797 because of the combined effect of the larger spatial TPW variation in the tropical region
798 than those in the mid-latitudes (see Fig. 1a, and Neiman et al., 2008; Teng et al., 2013;
799 Mears et al., 2015) and the fact that the MW TPW retrieval uncertainty is also larger over
800 stronger convection regions. More results are detailed in Section 4.

801 With a 0.25°×0.25° grid, there are about 20 to 60 MW pixels matching one
802 COSMIC observation. The number of pixels varies at different latitudes. A clear MW-RO
803 pair is defined as instances when *all* the TCW values for the collocated MW pixels are

Deleted: T

Deleted: those

806 equal to zero. A cloudy MW-RO ensemble is defined as instances when *all* the TCW values
807 from the collocated MW pixels are larger than zero. Partly cloudy conditions (some of
808 pixels zero and some non-zero) are excluded from this study. The cloudy ensembles are
809 further divided into precipitating and non-precipitating conditions. MW-RO pairs are
810 defined as cloudy non-precipitating when less than 20% of MW pixels have rainfall rates
811 larger than zero mm/hour. Cloudy precipitating MW-RO pairs are defined when more than
812 20% of the pixels have rainfall rates larger than zero. Because microwave radiances are not
813 sensitive to ice, we treat cloudy pixels of low density like cirrus clouds as clear pixels.

814 The matching pairs of RO and MW observations are not distributed uniformly over
815 the world oceans. In fact, they are heavily concentrated in middle latitudes, as shown in
816 Figure 1e. This biased distribution is caused by several factors, including the polar orbits
817 of the satellites, which produce more observations in higher latitudes, and also the failure
818 of many COSMIC RO soundings to penetrate to 0.1km in the subtropics and tropics (due
819 to super-refraction which is often present in these regions). Thus the results presented here,
820 especially the trends, are not representative of global averages. However, the main purpose
821 of this paper is to compare two independent satellite systems for obtaining TPW under
822 varying sky conditions. If the agreement is good, one has confidence in both systems. In
823 this case, SSM/I and WindSat estimates of TPW will be verified and then can be used with
824 confidence globally, including where RO observations are sparse or do not exist.

825

826 3. Comparison of MW and RO TPW with clear skies

827 In total there are 26,678 F15-RO pairs, 32,610 F16-RO pairs, 31,291 F17-RO pairs,
828 and 21,996 WindSat-RO pairs from June 2006 to December, 2013, respectively. Figures

Deleted: 1
Deleted: .
Deleted: Because microwave radiances are not sensitive to ice, we treat cloudy pixels of low density like cirrus clouds as clear pixels.

834 2a-d show scatter plots for F15-COSMIC TPW, F16-COSMIC TPW, F17-COSMIC TPW,
835 and WindSat-COSMIC TPW under clear skies. Figures 2a-d show that the MW clear sky
836 TPW from F15, F16, F17, and WindSat are all very consistent with those from co-located
837 COSMIC observations. As summarized in Table 2, under clear conditions where SSM/I
838 provides high quality TPW estimates, the mean TPW bias between F16 and COSMIC
839 (F16- COSMIC) is equal to 0.03 mm with a standard deviation σ of 1.47 mm. The mean
840 TPW differences are equal to 0.06 mm with a σ of 1.65 mm for F15, 0.07 mm with a σ of
841 1.47 mm for F17, and 0.18 mm with a σ of 1.35 mm for WindSat. The reason for larger
842 standard deviation for F15 may be because the F15 data after August 2006 were corrupted
843 by the “rad-cal” beacon that was turned on at this time (Hilburn and Wentz, 2008). On 14
844 August 2006, a radar calibration beacon (RAD-CAL) was activated on F15. This radar
845 interfered with the SSM/I, primarily the 22V channel, which is a key channel for water
846 vapor retrievals. Although a correction method derived by Hilburn and Wentz (2008) and
847 Hilburn (2009) was applied, the 22 V channel is not being full corrected (Wentz, 2012).
848 As a result, there are still errors in the water vapor retrievals. F16 had solar radiation
849 intrusion into the hot load during the time period, while F17 and WindSat had no serious
850 issues.

Deleted: 3

Deleted: es

851

852 4. Global comparisons of MW and RO TPW with cloudy skies

853 4.1 Comparison of MW, RO, and Ground-based GPS TPW

854 Figures 3a-c depict the scatter plots for F16-COSMIC pairs under cloudy, cloudy
855 non-precipitating, and precipitating conditions from June 2006 to December 2013 over
856 oceans. While there is a very small bias (0.031 mm) for clear pixels (Figure 2b), there is a

Deleted: on

Deleted: on

Deleted: .

§62 significant positive TPW bias (0.794 mm) under cloudy conditions (Figure 3a). This may
§63 explain the close to 0.45 mm mean TMI-gb GPS TPW biases found by Wentz et al., (2015)
§64 where a close to 7 years of data were used. Figure 3c depicts that the large SSM/I TPW
§65 biases under cloudy skies are mainly from the pixels with precipitation (mean bias is equal
§66 to 1.825 mm) although precipitation pixels are of about less than 6% of the total F16-
§67 COSMIC pairs. Because RO measurements are not significantly affected by clouds and
§68 precipitation, the biases mainly result from MW retrieval uncertainty under cloudy
§69 conditions. The fact that the MW-COSMIC biases for precipitating conditions (1.825 mm,
§70 Figure 3c and 1.64-1.88 mm in Table 2) is much larger than those for cloudy, but non-
§71 precipitating conditions, indicates that significant scattering and absorbing effects are
§72 present in the passive MW measurements when it rains. The correlation coefficients for
§73 F15-RO, F16-RO, F17-RO, and WindSat-RO pairs for all sky conditions are all larger than
§74 0.96 (not shown).

§75 MW and gb-GPS TPW comparisons show similar differences as the MW-RO
§76 differences under different sky conditions. We compared F16 pixels with those from gb-
§77 GPS within 50 km and 1 hour over the 33 stations studied by Mears et al. (2015) from 2002
§78 to 2013. Figures 4a-d depict the scatter plots for F16-gb-GPS TPW under clear, cloudy,
§79 cloudy non-precipitating, and cloudy precipitating conditions, respectively. The F16-gb-
§80 GPS mean biases are equal to 0.241 mm (clear skies), 0.614 mm (cloudy skies), 0.543 mm
§81 (cloudy-non precipitation) and 1.197 mm (precipitation), which are similar to those
§82 estimated from MW-RO comparisons (Table 2).

§83 The above results show that the MW estimates of TPW are biased positively
§84 compared to both the RO and the ground-based GPS estimates, which are independent

Deleted: on

Deleted: .

Deleted: 2

Deleted: on

Deleted: the

Deleted: s.

Deleted: s

892 measurements. The biases are smallest for clear skies and largest for precipitating
893 conditions, with cloudy, non-precipitating biases in between. Overall, the results suggest
894 that clouds and especially precipitation contaminate the MW radiometer measurements,
895 which in turn affect the MW TPW retrievals.

Deleted: to a small but significant degree.

Deleted: that

897 **4.2 Time Series of MW, RO, and Ground-based TPW Biases under Various** 898 **Meteorological Conditions**

899 To further examine how rain and cloud droplets affect the MW TPW retrievals, we
900 show how the F16-RO TPW biases vary under different meteorological conditions in
901 Figure 5. The bias dependence on wind speed (Figure 5a) is small. Unlike the results from
902 Mears et al., (2015), the mean TPW biases between F16 and COSMIC are within 0.5 mm
903 with high winds (wind speed larger than 20 m/s). Figure 5b indicates that the F16-COSMIC
904 bias is larger with TPW greater than about 10 mm, which usually occurs under cloudy
905 conditions. The F16-COSMIC biases can be as large as 2.0 mm when the rainfall rate is
906 larger than 1 mm/hour (Figure 5c), which usually occurs with high total liquid cloud water
907 conditions. The F16 TPW biases can be as large as 2 mm when total cloud water is larger
908 than 0.3 mm (Figure 5d). Figure 5e shows that the larger F16-COSMIC TPW biases (2-3
909 mm) mainly occur over regions with surface skin temperature less than 270 K (higher
910 latitudes, see Figure 1b). The F15, F17, and WindSat TPW biases under different
911 meteorological conditions are very similar to those of F16 (not shown).

Deleted: s

Deleted: (Fig. 5d)

912 In Figure 6 we compare RSS V7.0 F16 MW TPW to the ground-based GPS TPW
913 over various meteorological conditions. The magnitudes of the MW-gb-GPS TPW
914 differences under high rain rate and high total cloud water conditions are somewhat smaller

919 than those of MW-RO pairs (varying from about 0.5 mm to 2.0 mm), which may be because
920 most of the MW-gb-GPS samples are collected under low rain rates (less than 1 mm/hour)
921 conditions.

922

923 **5. Eight Year Time Series and Trend Analysis under All Skies**

924 **5.1 Monthly Mean TPW Time Series Comparison**

925 To further examine MW TPW long-term stability and trend uncertainty due to rain
926 and water droplets for different instruments, we compared time series of the MW and
927 COSMIC monthly mean TPW differences from June 2006 to December 2013. Figures 7a-
928 d show the monthly mean F16-COSMIC TPW differences from June 2006 to December
929 2013 for clear, cloudy, cloudy non-precipitating, and precipitating conditions. In general,
930 the microwave TPW biases under different atmospheric conditions are positive and stable
931 from June 2006 to December 2013, as reflected in relatively small standard deviation
932 values (Table 3). Except for F15, the standard deviations of the monthly mean TPW
933 anomaly range are less than 0.38 mm (Table 3). In contrast, the F15-COSMIC monthly
934 mean σ range from 0.48 mm to 0.69 mm with different conditions.

935 Table 3 also shows the trend in the RO estimates of TPW differences over the eight-
936 year period of study. The trends are range from -0.12 mm/decade (WindSat, clear skies) to
937 2.52 mm/decade (F15, precipitating conditions). The overall trend of TPW as estimated by
938 RO (second line in each row of Table 3) is positive as discussed in the next section. Table
939 3 shows that in general the trends are more strongly positive under cloudy and precipitating
940 conditions compared to clear conditions.

941

Deleted: on

Deleted: on

Deleted: on

Deleted: tion

946 **5.2 De-seasonalized Trends of MW-RO Differences and TPW**

947 Figure 8 depicts the de-seasonalized trends of the MW-RO TPW differences for
948 F15 (Figure 8a), F16 (Figure 8b), F17 (Figure 8c), and WindSat (Figure 8d) under cloudy
949 skies. Except for F15, the de-seasonalized trends of the MW-RO TPW differences for the
950 MW radiometers are close to zero, indicating little change over these eight years. The
951 trends of the biases associated with F15, F16, F17, and WindSat under all sky conditions
952 range from -0.09 to 0.27 mm/decade (details not shown).

953 The reason for larger standard deviations of the MW minus RO differences for F15
954 (Tables 2 and 3 and Figure 8a) is very likely because the F15 data after August 2006 were
955 corrupted by the “rad-cal” beacon that was turned on at this time. Adjustments were derived
956 and applied to reduce the effects of the beacon, but the final results still show excess noise
957 relative to uncorrupted measurements (Hilburn and Wentz, 2008). RSS does not
958 recommend using these measurements for studies of long-term change. Thus we consider
959 the F15 data less reliable during the period of our study.

960 Figure 9 shows the de-seasonalized time series of the monthly mean TPW for all
961 MW and RO pairs under all sky conditions. The close to eight year trends for TPW
962 estimated from both passive MW radiometers and active COSMIC RO sensors are positive
963 and very similar in magnitude. The mean trend of all COSMIC RO TPW is 1.79
964 mm/decade with a 95% confidence interval of (0.96, 2.63) mm/decade while the mean
965 trend from all the MW estimates is 1.78 mm/decade with a 95% confidence interval of
966 (0.94, 2.62). This close agreement between completely independent measurements lends
967 credence to both estimates. The mean TPW over this period, calculated from all MW data

Deleted: under cloudy skies

Deleted: s

Deleted: 6

Deleted: 7

Deleted: 8

Deleted:

Deleted: global

Deleted: radiometers and COSMIC

Deleted: global

Deleted: global

978 in our data set was 26.04 mm; thus the trend of 1.78 mm/decade represents a trend of
979 approximately 6.9% per decade for our data set.

980 As discussed earlier, the trend of 1.78 mm/decade is heavily biased toward middle
981 latitudes (40°N-60°N and 40°-65°S) and is not representative of a global average. In fact,
982 it is four to six times larger than previous estimates over earlier time periods. For example,
983 Durre et al. (2009) estimated a trend of 0.45 mm/decade for the Northern Hemisphere over
984 the period 1973-2006. Trenberth et al. (2005) estimated a global trend of 0.40 +/- 0.09
985 mm/decade for the period 1988 to 2001. Using SSM/I data, Wentz et al. (2007) estimated
986 and an increase of 0.354 mm/decade over the period 1997-2006. The 100-year trend in
987 global climate models is variable, ranging from 0.55 to 0.72 mm/decade (Roman et al.,
988 2014).

989 The very close agreement between RO and MW observations where they co-exist
990 gives credibility to both observing systems and allows us to use global MW data to compute
991 global TPW trends over all oceanic regions, including where RO observations are sparse
992 or absent. Figure 10 shows the global map of TPW trends over oceans using all F16, F17,
993 and WindSat data from 2006 to 2013. Figure 10 shows that the positive trends in TPW
994 occur mainly over the central and north Pacific, south of China and west of Australia,
995 south-east of South America, and east of America. Positive trends also exist in general
996 over the middle latitudes (40°N-60°N and 40°-65°S) where most of our matching RO and
997 MW data pairs occur.

998 Mears et al. (2017) computed global average (60°S to 60°N) TPW using a number
999 of data sets from 1979 to 2014. Figure 11 shows the data from the ERA-Interim reanalysis
1000 (Dee et al. 2011), RSS MW, and COSMIC. (This figure was obtained using the same data

Deleted: .

Deleted: exist

Deleted: oceans

Deleted: n

Deleted: n

Deleted:

1007 used to construct Figure 2.16 in Mears et al., 2017). Fig. 11 shows close agreement between
1008 RSS MW and COSMIC. The global mean trend from June 2006 to December 2013 from
1009 the COSMIC observations is 0.32 mm/decade and for RSS MW it is 0.31 mm/decade.
1010

1011 **6. Conclusions and Discussions**

1012 RSS water vapor products have been widely used for climate research. The newly
1013 available RSS V7.0 data products have been processed using consistent calibration
1014 procedures (Wentz, 2013). This was done for the explicit purpose of producing versions of
1015 the datasets that can be used to study decadal scale changes in TPW, wind, clouds, and
1016 precipitation. These water vapor products are mainly verified by comparing to either
1017 reanalyses, radiosondes measurements, or other satellite data. However, because the
1018 quality of these datasets may also vary under different atmospheric conditions, the
1019 uncertainty in long-term water vapor estimates may still be large. In this study, we used
1020 TPW estimates derived from COSMIC active RO sensors to identify TPW uncertainties
1021 from four different MW radiometers under clear, cloudy, cloudy/non-precipitating, and
1022 cloudy/precipitating skies over nearly eight years (from June 2006 to December 2013).
1023 Because RO data have low sensitivity to clouds and precipitation, RO-derived water vapor
1024 products are useful to identify the possible TPW biases retrieved from measurements of
1025 passive microwave imagers under different sky conditions. We reach the following
1026 conclusions:

1027 1) Clear sky biases: The collocated COSMIC RO TPW estimates under clear skies
1028 are highly consistent with the MW TPW estimates under clear sky conditions (within +/-
1029 0.2 mm and with a correlation coefficient greater than 0.96). The mean TPW bias between

Deleted: Discussion and
Deleted: c

Deleted: i

Deleted: on

Deleted: on

Deleted: are

Deleted: not

Deleted: sensitiv

Deleted: e

1039 F16 and COSMIC (F16- COSMIC) is equal to 0.03 mm with a standard deviation σ of 1.47
1040 mm. The mean TPW differences are equal to 0.06 mm with a σ of 1.65 mm for F15, 0.07
1041 mm with a σ of 1.47 mm for F17, and 0.18 mm with a σ of 1.35 mm for WindSat. The
1042 consistent F15-COSMIC, F16-COSMIC, F17-COSMIC, and WindSat-COSMIC TPW
1043 under clear skies show that COSMIC TPW can be used as reliable reference data to identify
1044 and correct TPW among different MW imagers for other sky conditions.

Deleted: also
Deleted: good
Deleted: s

1045 2) Biases under cloudy skies: While there are very small biases for clear pixels,
1046 there are significant positive MW TPW biases (~0.80 mm) under cloudy conditions when
1047 compared to RO TPW. The large SSM/I TPW biases under cloudy skies result mainly from
1048 the pixels with precipitation. The mean bias is equal to 1.83 mm for COSMIC-F16 pairs,
1049 which is much larger than the bias for cloudy, but non-precipitating conditions. This
1050 indicates that the significant scattering and absorbing effects are present in the passive MW
1051 measurements when it rains. The F16 – Ground-based GPS mean biases are equal to 0.24
1052 mm (for clear skies), 0.61 mm (for cloudy skies), 0.54 mm (for cloudy/non-precipitating
1053 skies) and 1.2 mm (for precipitating skies) which are consistent with those from F16-
1054 COSMIC comparisons.

Deleted: w

Deleted: on

Deleted: on
Deleted: on

1055 3) Biases among different instruments: Using RO TPW estimates collocated with
1056 different MW instruments, we are able to identify possible TPW inconsistencies among
1057 MW instruments even they are not collocated. The de-seasonalized trends in MW-RO TPW
1058 differences for three MW radiometers (i.e., F16, F17, and WindSat) are close to zero,
1059 indicating consistency among these radiometers. However, the F15-COSMIC differences
1060 are larger and show a significant trend over the eight years of the study. It is likely that F15

Deleted: u

1069 data after August 2006 were corrupted by the “rad-cal” beacon that was turned on at this
1070 time.

1071 4) Trend of TPW under all skies: The eight-year trends of TPW estimated from
1072 both passive MW radiometer and active COSMIC sensors in our data set show increasing
1073 TPW, with slightly higher trends under cloudy conditions. The mean trend of COSMIC
1074 RO TPW collocated with MW observations in our data set is 1.79 mm/decade with a 95%
1075 confidence interval of (0.96, 2.63) mm/decade. The corresponding mean trend from all the
1076 MW estimates is 1.78 mm/decade with a 95% confidence interval of (0.94, 2.62). The mean
1077 trend from all the MW estimates under cloudy conditions is 1.93 mm/decade with a 95%
1078 confidence interval of (0.97, 2.89). The mean trend from all the COSMIC RO TPW
1079 estimates under cloudy conditions is 1.82 mm/decade with a 95% confidence interval of
1080 (0.88, 2.76). These increases represent about a 6.9% per decade increase in the mean TPW
1081 of our data set. The close agreement between completely independent measurements lends
1082 credence to both estimates.

1083 The trends of TPW in our data set, which are heavily biased toward middle latitudes
1084 (40°N-60°N and 40°S-65°S) are higher than previous global estimates over earlier time
1085 periods by about a factor of four to six. As also shown by the regional distribution of TPW
1086 trends estimated from the MW observations, the large positive trends in these latitudes,
1087 which are the main latitudes of extratropical storm tracks, are a strong confirmation of the
1088 water vapor-temperature feedback in a warming global atmosphere particularly under
1089 cloudy conditions.

1090 Other studies have suggested that this positive feedback results in a nearly constant
1091 global mean relative humidity (Soden and Held, 2006; Sherwood et al., 2010). However,

Comment [RA1]:

Deleted: globally

Deleted: global

Deleted: global

Deleted: global

Deleted: global

Deleted: global

Deleted: is

Deleted: Note that t

Deleted: se

Deleted: are significantly

Deleted: other

Deleted: and

Formatted: Not Highlight

Deleted: over vert

1105 it is difficult to directly relate our estimated TPW trends to constant RH hypothesis of
1106 Earth's atmosphere under global warming. The global mean surface temperature has been
1107 rising at about the rate of 0.2 K/decade in the past twenty years. A 0.2K increase in
1108 temperature would produce about a 1.4% increase in saturation water vapor pressure based
1109 on the Clausius-Clapeyron equation. To maintain a constant RH for this temperature
1110 increase, the actual water vapor pressure (and specific humidity) would also have to
1111 increase by 1.4%. In this study, we observe an increase of TPW in our dataset of about 1.78
1112 mm/decade which is 6.9 percent increase per decade in TPW. Our dataset is dominated
1113 mainly by cloudy samples over middle latitudes (40°N-60°N and 40°-65°S). Thus, from
1114 these numbers alone we would expect an increase in mean RH under cloudy conditions by
1115 more than 6%, which is unlikely and well outside the range of changes in relative humidity
1116 in models (e.g. Figure 2 in Sherwood et al., 2010). However, the changes in the global
1117 mean RH are not related in such a simple fashion to changes in the global mean temperature
1118 and precipitable water. For example, Figure 10 depicts that there are very large differences
1119 in the spatial distribution of TPW changes, which shows regional variations of +/- 4
1120 mm/decade. Thus, some regions are drying and others are moistening. The variations in
1121 global mean surface temperature are also large, but very different from those of TPW, with
1122 the polar regions and continents warming up much faster than the atmosphere over the
1123 oceans. In cold polar regions, an increase in temperature will result in a smaller increase in
1124 saturation vapor pressure than the same increase in temperature in the tropics. The global
1125 evaporation and precipitation patterns also vary greatly, as water vapor transport is
1126 important in the global water vapor balance. All of this, as discussed by Held and Soden
1127 (2000), Soden and Held (2006), and Sherwood et al. (2010) means that the relationships

1128 between global mean temperature increase, TPW changes, and the resulting change in
1129 global mean RH are not simple.

1130

1131 **Acknowledgements.** This work is supported by the NSF CAS AGS-1033112. We thank
1132 Eric DeWeaver (NSF) and Jack Kaye (NASA) for sponsoring this work.

1133

1134

1135

1136

1137

1138

1139

1140

1141

1142

1143

1144

1145

1146

1147

1148

1149

1150

1151 **References**

- 1152 Anthes, R. A., P. Bernhardt, Y. Chen, L. Cucurull, K. Dymond, D. Ector, S. Healy, S.-P.
1153 Ho, D. Hunt, Y.-H. Kuo, H. Liu, K. Manning, C. McCormick, T. Meehan, W. Randel,
1154 C. R. Rocken, W. Schreiner, S. Sokolovskiy, S. Syndergaard, D. Thompson, K.
1155 Trenberth, T.-K. Wee, Z. Zeng, 2008: The COSMIC/FORMOSAT-3 Mission: Early
1156 Results, *Bul. Amer. Meteor. Sci.* 89, No.3, 313-333, DOI: 10.1175/BAMS-89-3-313.
- 1157 Anthes, R.A., 2011: Exploring Earth's atmosphere with radio occultation: contributions to
1158 weather, climate and space weather. *Atmos. Meas. Tech.*, 4, 1077-1103,
1159 DOI:10.5194/amt-4-1077-2001.
- 1160 Biondi, R., W. Randel, S.-P. Ho, T. Neubert, and S. Syndergaard, 2012: Thermal
1161 structure of intense convective clouds derived from GPS radio occultations. *Atmos.*
1162 *Chem. Phys.*, doi:10.5194/acp-12-5309-2012.
- 1163 Biondi, R., S.-P. Ho, W. Randel, T. Neubert and S. Syndergaard, 2013: Tropical cyclone
1164 cloud-top heights and vertical temperature structure detection using GPS radio
1165 occultation measurements, *J. Geophys. Research*, VOL. 118, 1–13,
1166 doi:10.1002/jgrd.50448.
- 1167 Bock, O., Bosser, P., Bourcy, T., David, L., Goutail, F., Hoareau, C., Keckhut, P.,
1168 Legain, D., Pazmino, A., Pelon, J., Pipis, K., Poujol, G., Sarkissian, A., Thom, C.,
1169 Tournois, G., and Tzanos, D. 2013: Accuracy assessment of water vapour
1170 measurements from in situ and remote sensing techniques during the DEMEVAP
1171 2011 campaign at OHP, *Atmos. Meas. Tech.*, 6, 2777–2802, doi:10.5194/amt-6-
1172 2777-2013.
- 1173 Cober, S. G., G. A. Isaac, and J. W. Strapp, 2001: Characterizations of aircraft icing

1174 environments that include supercooled large drops. *J. Appl. Meteor.*, 40, 1984–2002.

1175 Durre, I., C. N. Williams Jr., X. Yin, and R. S. Vose, 2009: Radiosonde-based trends in
1176 precipitable water over the Northern Hemisphere: An update, *J. Geophys. Res.*, 114,
1177 D05112, doi:10.1029/2008JD010989.

1178 [Dee D.P., S.M. Uppala, A.J. Simmons, P. Berrisford, P. Poli, S. Kobayashi, U. Andrae,](#)
1179 [M.A. Balmaseda, G. Balsamo, P. Bauer, P. Bechtold, A.C.M. Beljaars, L. van de](#)
1180 [Berg, J. Bidlot, N. Bormann, C. Delsol, R. Dragani, M. Fuentes, A.J. Geer, L.](#)
1181 [Haimberger, S.B. Healy, H. Hersbach, E.V. Hölm, L. Isaksen, P. Kållberg, M.](#)
1182 [Köhler, M. Matricardi, A.P. McNally, B.M. Monge-Sanz, J.-J. Morcrette, B.-K.](#)
1183 [Park, C. Peubey, P. de Rosnay, C. Tavalato, J.-N. Thepaut, and F. Vitart](#), 2011: The
1184 ERA-Interim reanalysis: configuration and performance of the data assimilation
1185 system. *Q. J. R. Meteorol. Soc.* **137**: 553–597. DOI:10.1002/qj.828

1186 Elsaesser, G. S. and C. D. Kummerow, 2008: Towards a fully parametric retrieval of the
1187 non-raining parameters over the global ocean. *J. Appl. Meteor. & Climatol.*, 47, 1590
1188 – 1598.

1189 Fetzer, E. J., B. H. Lambrigtsen, A. Eldering, H. H. Aumann, and M.T. Chahine, M.T.,
1190 2006: Biases in total precipitable water vapor climatologies from atmospheric infrared
1191 sounder and advanced microwave scanning radiometer. *J. Geophys. Res.*, 111,
1192 D09S16, doi: 10.1029/2005JD006598.

1193 Fetzer, E. J., W.G. Read, D. Waliser, [B. H. Kahn, B. Tian, H. Vömel, F. W. Irion, H. Su,](#)
1194 [A. Eldering, M. T. Juarez, J. Jiang, and V. Dang.](#) 2008: Comparison of upper
1195 tropospheric water vapor observations from the Microwave Limb Sounder and
1196 Atmospheric Infrared Sounder. *J. Geophys. Res.*, 113/D22, D22110.

1197 [Held, I. M., and B. J. Soden, 2000: Water vapor feedback and global warming, *Annu. Rev.*](#)
1198 [Energy Environ., 25, 441–475, doi:10.1146/annurev.energy.25.1.441.](#)

1199 [Heymsfield, A. J., A. Bansemer, P. R. Field, S. L. Durden, J. L. Stith, J. E. Dye, W. Hall,](#)
1200 [and C. A. Grainger, 2002: Observations and parameterizations of particle size](#)
1201 [distributions in deep tropical cirrus and stratiform precipitating clouds: Results from in](#)
1202 [situ observations in TRMM field campaigns. *J. Atmos. Sci.*, 59, 3457–3491,](#)
1203 [doi:10.1175/1520-0469\(2002\)059, 3457.](#)

1204 [Hilburn, K.A., 2009: Including temperature effects in the F15 RADCAL Beacon](#)
1205 [correction. RSS Technical Report 051209, Remote Sensing Systems, Santa Rosa, CA.](#)
1206 [http://www.remss.com/papers/RSS_TR051209_RADCAL.pdf.](http://www.remss.com/papers/RSS_TR051209_RADCAL.pdf)

1207 Hilburn, K. A., F. J. Wentz, 2008: Mitigating the impact of RADCAL beacon
1208 contamination on F15 SSM/I ocean retrievals, *Geophysical Research Letters*, 35,
1209 L18806, doi:10.1029/2008GL034914.

1210 Ho, S.-P., Kuo, Y.-H., and Sokolovskiy, S., 2007: Improvement of the temperature and
1211 moisture retrievals in the lower troposphere using AIRS and GPS radio occultation
1212 measurements. *J. Atmos. Oceanic Technol.*, 24, 1726-1739,
1213 doi:10.1175/JTECH2071.1.

1214 Ho, S.-P., G. Kirchengast, S. Leroy, J. Wickert, A. J. Mannucci, A. K. Steiner, D. Hunt,
1215 W. Schreiner, S. Sokolovskiy, C. O. Ao, M. Borsche, A. von Engeln,
1216 U. Foelsche, S. Heise, B. Iijima, Y.-H. Kuo, R. Kursinski, B. Pirscher, M. Ringer, C.
1217 Rocken, and T. Schmidt, 2009a: Estimating the Uncertainty of using GPS Radio
1218 Occultation Data for Climate Monitoring: Inter-comparison of CHAMP Refractivity
1219 Climate Records 2002-2006 from Different Data Centers, *J. Geophys.*

1220 *Res.*, doi:10.1029/2009JD011969.

1221 Ho, S.-P., M. Goldberg, Y.-H. Kuo, C.-Z. Zou, W. Schreiner, 2009b: Calibration of
1222 Temperature in the Lower Stratosphere from Microwave Measurements using
1223 COSMIC Radio Occultation Data: Preliminary Results, *Terr. Atmos. Oceanic Sci.*,
1224 Vol. 20, doi: 10.3319/TAO.2007.12.06.01(F3C).

1225 Ho, S.-P., Y.-H. Kuo, W. Schreiner, X. Zhou, 2010a: Using SI-traceable Global Positioning
1226 System Radio Occultation Measurements for Climate Monitoring [In “States of the
1227 Climate in 2009]. *Bul. Amer. Meteor. Sci.*, 91 (7), S36-S37.

1228 Ho, S.-P., Zhou X., Kuo Y.-H., Hunt D., Wang J.-H., 2010b: Global Evaluation of
1229 Radiosonde Water Vapor Systematic Biases using GPS Radio Occultation from
1230 COSMIC and ECMWF Analysis. *Remote Sensing*. 2010; 2(5):1320-1330.

1231 Ho, S.-P., D. Hunt, A. K. Steiner, A. J. Mannucci, G. Kirchengast, H. Gleisner, S. Heise,
1232 A. von Engeln, C. Marquardt, S. Sokolovskiy, W. Schreiner, B. Scherllin-Pirscher,
1233 C. Ao, J. Wickert, S. Syndergaard, K. B. Lauritsen, S. Leroy, E. R. Kursinski, Y.-H.
1234 Kuo, U. Foelsche, T. Schmidt, and M. Gorbunov, 2012: Reproducibility of GPS
1235 Radio Occultation Data for Climate Monitoring: Profile-to-Profile Inter-comparison
1236 of CHAMP Climate Records 2002 to 2008 from Six Data Centers, *J. Geophys.*
1237 *Research*. VOL. 117, D18111, doi:10.1029/2012JD017665.

1238 Huang, C.-Y., W.-H. Teng, S.-P. Ho, Y.-H. Kuo, 2013: Global Variation of COSMIC
1239 Precipitable Water over Land: Comparisons with Ground-based GPS Measurements
1240 and NCEP Reanalyses, *Geophysical Research Letters*, DOI: 10.1002/grl.50885.

1241 IPCC, 2013: Climate Change 2013: The Physical Science Basis. Contribution of Working
1242 Group I to the Fifth Assessment Report of the Intergovernmental Panel on Climate

1243 Change (IPCC). Cambridge University Press, Cambridge, United Kingdom and New
1244 York, NY, USA, 1535 pp, doi:10.1017/CBO9781107415324.

1245 John, V. O. and B.J. Soden, 2007: Temperature and humidity biases in global climate
1246 models and their impacts on climate feedbacks. *Geophysical Research Letters*, 34,
1247 L18605, doi:10.1029/2007GL030736.

1248 Knuteson, R., S. Bedka, J. Roman, D. Tobin, D. Turner, and H. Revercomb, 2010: AIRS
1249 and IASI Precipitable Water Vapor (PWV) Absolute Accuracy at Tropical, Mid-
1250 Latitude, and Arctic Ground-Truth Sites. Presented at the International TOVS Study
1251 Conference, Monterey, CA, USA, 14-10 April 2010, available online at
1252 <http://cimss.ssec.wisc.edu/itwg/itsc/itsc17/>.

1253 Kursinski, E.R., G.A. Hajj, J.T. Schofield and R.P. Linfield, 1997: Observing Earth's
1254 atmosphere with radio occultation measurements using the Global Positioning
1255 System. *J. Geophys. Res.* 102, No. D19, 23,429-23,465.

1256 Larar, A. M., W. L. Smith, D. K. Zhou, X. Liu, H. Revercomb, J. P. Taylor, S. M. Newman,
1257 and P. Schlüssel, 2010: IASI spectral radiance validation inter-comparisons: case study
1258 assessment from the JAIVEx field campaign, *Atmos. Chem. Phys.*, 10, 411-430.

1259 [Leroy, D., Fontaine, E., Schwarzenboeck, A., Strapp, J. W., Korolev, A., McFarquhar, G.,
1260 Dupuy, R., Gourbeyre, C., Lilie, L., Protat, A., Delanoë, J., Dezitter, F., and Grandin,
1261 A., 2017: Ice crystal sizes in high ice water content clouds. Part 2: Statistics of mass
1262 diameter percentiles in tropical convection observed during the HAIC/HIWC project,
1263 *J. Atmos. Oceanic Technol.*, doi: 10.1175/JTECH-D-15-0246.1.](#)

1264 Lin, L., X. Zou, R. Anthes, and Y.-H. Kuo, 2010: COSMIC GPS cloudy profiles. *Mon.*
1265 *Wea. Rev.*, 138, 1104–1118.

1266 Luers, J. K. and R.E. Eskridge, 1998: Use of radiosonde temperature data in climate
1267 studies. *J. of Climate*, 11, 1002–1019.

1268 Ma, Z., Y.-H. Kuo, F. M. Ralph, P. J. Neiman, G. A. Wick, E. Sukovich, and B. Wang,
1269 2011: Assimilation of GPS radio occultation data for an intense atmospheric river
1270 with the NCEP regional GSI system. *Mon. Wea. Rev.*, 139, 2170–2183,
1271 doi:10.1175/2011MWR3342.1.

1272 Mears, C., J. Wang, S.-P. Ho, L. Zhang, and X. Zhou, 2012: Global Climate Hydrological
1273 cycle, Total column water vapor [in “State of the Climate in 2011”]. *Bull. Amer.*
1274 *Meteor. Soc.*, 93(7), S25–S26, doi:10.1175.

1275 Mears, C., J. Wang, D. Smith, and F. J. Wentz, 2015: Intercomparison of total precipitable
1276 water measurements made by satellite- borne microwave radiometers and ground-
1277 based GPS instruments. *J. Geophys. Res. Atmos.*, 120, 2492–2504,
1278 doi:10.1002/2014JD022694.

1279 [Mears C., S.-P. Ho, L. Peng, and J. Wang, 2017\): Total Column Water Vapor, \[In “State](#)
1280 [of the Climate in 2016\]. *Bul. Amer. Meteor. Sci.*, 98 \(8\), S93–S98,](#)
1281 [doi:10.1175/2017BAMSStateoftheClimate.1.](#)

1282 Milz, M., S. A. Buehler, and V. O. John, 2009: Comparison of AIRS and AMSU-B
1283 monthly mean estimates of upper tropospheric humidity, *Geophys. Res. Lett.*, L10804,
1284 doi:10.1029/2008GL037068.

1285 Neiman, P. J., F. M. Ralph, G. A. Wick, Y.-H. Kuo, T.-K. Wee, Z. Ma, G. H. Taylor, and
1286 M. D. Dettinger, 2008: Diagnosis of an intense atmospheric river impacting the Pacific
1287 Northwest: Storm summary and offshore vertical structure observed with COSMIC
1288 satellite retrievals. *Mon. Wea. Rev.*, 136, 4398–4420.

1289 Noël, S., M. Buchwitz, and J. P. Burrows, 2004: First retrieval of global water vapour
1290 column amounts from SCIAMACHY measurements, *Atmos. Chem. Phys.*, 4, 111–
1291 125.

1292 Palm, M., C. Melsheimer, S. Noel, J. Notholt, J. Burrows, and O. Schrems, 2008: Integrated
1293 water vapor above Ny Alesund, Spitsbergen: a multisensor intercomparison. *Atmos.*
1294 *Chem. Phys. Discuss.* 8, 21171–21199.

1295 Pougatchev, N., T. August, X. Calbet, T. Hultberg, O. Oduleye, P. Schlüssel, B. Stiller, K.
1296 St. Germain, and G. Bingham, 2009: IASI temperature and water vapor retrievals –
1297 error assessment and validation. *Atmos. Chem. Phys.*, 9, 6453–6458.

1298 Prasad, A. K. and R. P. Singh, 2009: Validation of MODIS Terra, AIRS, NCEP/DOE
1299 AMIP-II Reanalysis-2, and AERONET Sun photometer derived integrated precipitable
1300 water vapor using ground-based GPS receivers over India. *J. Geophys. Res.*, 114,
1301 D05107, doi:10.1029/2008JD011230.

1302 Roman, J., R. Knuteson, and S. Ackerman, 2014: Time-to-detect trends in precipitable
1303 water vapor with varying measurement errors. *J. Climate*, 27, 8259-8275.

1304 Scherllin-Pirscher, B., C. Deser, S.-P. Ho, C. Chou, W. Randel, and Y.-W. Kuo, 2012:
1305 The vertical and spatial structure of ENSO in the upper troposphere and lower
1306 stratosphere from GPS radio occultation measurements, *Geophys. Res. Lett.*, 39,
1307 L20801, 6 PP., 2012, doi:10.1029/2012GL053071.

1308 Schliessel, P., & Emery, W. J. 1990: Atmospheric water vapour over oceans from SSM/I
1309 measurements. *International Journal of Remote Sensing*, 11(5), 753-766.

1310 [Sherwood, S.C., W. Ingram, Y. Tsushima, M. Satoh, M. Roberts, P.L. Vidale and P.A.O.](#)
1311 [Gorman, 2010: Relative humidity changes in a warmer climate. *J. Geophys. Res.*,](#)
1312 [115, D09104, doi:10.1029/2009JD012585.](#)

1313 Soden, B. J., and J. R. Lanzante, 1996: An assessment of satellite and radiosonde
1314 climatologies of upper-tropospheric water vapor. *Journal of Climate*, 9(6), 1235-
1315 1250.

1316 Soden, B. J., R. T. Wetherald, G. L. Stenchikov, and A. Robock, 2002: Global cooling after
1317 the eruption of Mount Pinatubo: A test of climate feedback by water
1318 vapor. *Science*, 296(5568), 727-730.

1319 Sohn, B. J., and E. A. Smith, 2003: Explaining sources of discrepancy in SSM/I water
1320 vapor algorithms. *J. Climate*, 16, 3229–3255, doi:10.1175/1520-
1321 0442(2003)016,3229:ESODII.2.0.CO;2.

1322 [Soden, B.J. and I.M. Held, 2006: Assessment of climate feedbacks in coupled ocean-](#)
1323 [atmosphere models. *J. Climate*, 19, 3354-3360.](#)

1324 Sohn, B.-J., and R. Bennartz, 2008: Contribution of water vapor to observational estimates
1325 of longwave cloud radiative forcing, *J. Geophys. Res.*, 113, D20107,
1326 doi:10.1029/2008JD010053.

1327 Teng, W.-H., C.-Y. Huang, S.-P. Ho, Y.-H. Kuo, and X.-J. Zhou, 2013: Characteristics of
1328 Global Precipitable Water in ENSO Events Revealed by COSMIC Measurements,
1329 *J. Geophys. Research*, Vol. 118, 1–15, doi:10.1002/jgrd.50371.

1330 Thompson, A., 2007: Simulating the adiabatic ascent of atmospheric air parcels using the
1331 cloud chamber, Department of Meteorology, Penn State.

1332 Trenberth K. E. and Guillemot, C. J., 1998: Evaluation of the atmospheric moisture and

1333 hydrological cycle in the NCEP/NCAR reanalyses. *Clim. Dyn.*, 14:213–231

1334 Trenberth, K.E., J. Fasullo, and L. Smith, 2005: Trends and variability in column

1335 integrated atmospheric water vapor. *Climate Dynamics*, 24, 741–758.

1336 Wang, J., L. Zhang, A. Dai, T. Van Hove, and J. Van Baelen, 2007: A near-global, 8-year,

1337 2-hourly data set of atmospheric precipitable water from ground-based GPS

1338 measurements. *J. Geophys. Res.*, 112, D11107, doi:10.1029/2006JD007529.

1339 Wang, J and Zhang L. 2008: Systematic Errors in Global Radiosonde Precipitable Water

1340 Data from Comparisons with Ground-Based GPS Measurements, *J. of Climate*, 21,

1341 DOI:10.1175/2007JCLI1944.1.

1342 Wang, L., X. Wu, M. Goldberg, C. Cao, Y. Li, and S.-H. Sohn, 2010: Comparison of AIRS

1343 and IASI Radiances Using GOES Imagers as Transfer Radiometers toward Climate

1344 Data Records. *J. Appl. Meteor. Climatol.* 49, 478–492.

1345 Wick, G.A., Kuo, Y.-H., Ralph, F.M., Wee, T.-K., Neiman, P.J., Ma, Z, 2008:

1346 Intercomparison of integrated water vapor retrievals from SSM/I and

1347 COSMIC. *Geophys. Res. Lett.* 2008, 28, 3263–3266.

1348 Wentz, F. J., 1997: A well-calibrated ocean algorithm for SSM/I. *J. Geophys.*

1349 *Res.*, 102, 8703–8718.

1350 Wentz, F. J., and R. W. Spencer, 1998: SSM/I rain retrievals within a unified all-weather

1351 ocean algorithm. *J. Atmos. Sci.*, 56, 1613–1627.

1352 [Wentz, F. J., and M. Schabel, 2000: Precise climate monitoring using complementary](#)

1353 [satellite data sets, *Nature*, 403, 414–416.](#)

1354 [Wentz, F.J., Lucrezia Riccardulli, K. Hilburn, and C. Mears, 2007: How much more rain](#)

1355 [will global warming bring? *Science*, 317, 233-235.](#)

1356 Wentz, F. J., 2013: SSM/I version-7 calibration report. *Remote Sensing Systems Tech.*
1357 Rep. 011012, 46 pp.

1358 Wentz, F. J. 2015: A 17-Year climate record of environmental parameters derived from
1359 the Tropical Rainfall Measuring Mission (TRMM) microwave imager, *J. Clim.*,
1360 doi:10.1175/JCLI-D-15-0155.1.

1361 Yang, S., and X. Zou, 2012: Assessments of cloud liquid water contributions to GPS RO
1362 refractivity using measurements from COSMIC and CloudSat. *J. Geophys. Res.*,
1363 117, D06219, doi:10.1029/2011JD016452.

1364 Zeng, Z., S.-P. Ho, S. Sokolovskiy, 2012: The Structure and Evolution of Madden-Julian
1365 Oscillation from FORMOSAT-3/COSMIC Radio Occultation Data, *J. Geophys.*
1366 *Research*, 117, D22108, doi:10.1029/2012JD017685.

1367 Zou, X., S. Yang, and P. S. Ray, 2012: Impacts of ice clouds on GPS radio occultation
1368 measurements. *J. Atmos. Sci.*, 69, 3670–3682.

1369

1370

1371

1372

1373

1374

1375

1376

1377

1378

1379

1380

1381 Table 1. Satellite Instruments Used in This Study

1382

Satellite	Instrument	Operation period
DMSP F15	SSM/I	December 1999-present
DMSP F16	SSMIS	October 2003-present
DMSP F17	SSMIS	December 2006-present
Coriolis	WindSat	February 2003-present

1383

1384

1385

1386

1387

1388

1389

1390

1391

1392

1393

1394

1395

1396

1397

1398

1399

1400
1401
1402
1403
1404
1405
1406
1407
1408
1409
1410
1411
1412
1413
1414
1415
1416
1417
1418
1419
1420
1421
1422
1423
1424
1425
1426
1427
1428
1429
1430
1431
1432
1433
1434
1435
1436
1437
1438
1439
1440
1441
1442

Table 2: Mean and standard deviation of differences (MW minus RO) in TPW (in mm) between four MW radiometers and COSMIC RO under various sky conditions. The sample numbers for each pair are shown in the third position of each column.

Sky condition	Mean/ σ /N			
	F15	F16	F17	WindSat
Clear	0.06/1.65/3064	0.03/1.47/3551	0.07/1.47/2888	0.18/1.35/1802
Cloudy	0.80/1.92/23614	0.79/1.73/29059	0.82/1.76/28403	0.96/1.73/20194
Non Precip	0.49/1.69/17223	0.46/1.46/21854	0.47/1.49/21371	0.49/1.36/13004
Precip	1.64/2.28/6391	1.83/2.05/7205	1.88/2.08/7032	1.85/2.00/7190

1443
 1444
 1445
 1446
 1447
 1448
 1449
 1450
 1451
 1452
 1453
 1454
 1455
 1456

Table 3: Mean and standard deviation (std) of the mean in mm of the monthly time series of differences of MW minus RO TPW under various sky conditions. The trend of the RO estimates of TPW in mm/decade and the 95% confidence level are shown below the mean and σ values in each row.

Sky condition	Mean/ σ of monthly time series RO trend (95% confidence levels indicated in ())			
	F15	F16	F17	WindSat
Clear	0.07/0.56 1.65 (0.47,2.84)	0.05/0.28 1.09 (-0.28,2.46)	0.08/0.27 0.21 (-1.22,1.65)	0.23/0.38 -0.12 (-1.89,1.66)
Cloudy	0.77/0.51 1.49 (0.40,2.58)	0.78/0.18 2.02(0.87,3.16)	0.82/0.15 1.85 (0.64,3.06)	0.95/0.17 1.85 (0.68,3.01)
Non Precipitation	0.46/0.48 0.86 (-0.24,1.95)	0.45/0.17 2.02 (0.87,3.17)	0.48/0.15 2.37 (1.23,3.50)	0.47/0.19 2.12 (0.95,3.30)
Precipitation	1.62/0.69 2.52 (0.55,4.48)	1.81/0.31 1.32 (-0.53,3.17)	1.88/0.29 0.26 (-1.59,2.10)	1.88/0.32 0.39 (-1.25,2.04)

1457
 1458
 1459

 1460

 1461

 1462
 1463
 1464
 1465
 1466
 1467
 1468
 1469

1470
1471 Figure Captions

1472
1473 Figure 1. a.-e: The RSS V7.0 monthly mean F16 SSM/I a) TPW (in mm), b) surface skin
1474 temperature (in K), c) liquid water path (LWP, in mm), and d) rain rate (RR, in
1475 mm/hour), and e) distribution of matches of COSMIC RO and F16, F17, and WindSat
1476 estimations of TPW used in this study.

1477
1478 Figure 2. TPW scatter plots for the COSMIC and RSS Version 7.0 pairs under clear
1479 conditions for a) F15, b) F16, c) F17, and d) WindSat.

1480
1481 Figure 3. TPW scatter plots for the COSMIC and RSS Version 7.0 F16 SSM/I pairs
1482 under a) cloudy, b) cloudy but non-precipitation, and c) precipitation conditions.

1483
1484 Figure 4. TPW scatter plots for the gb-GPS and RSS Version 7.0 F16 SSM/I pairs from
1485 June 2006 to December 2013 under a) clear, b) cloudy, c) cloudy but non-precipitation,
1486 and d) precipitation conditions.

1487
1488 Figure 5. Mean and standard of the mean for the F16-COSMIC TPW biases varying with
1489 a) wind speed (m/s), b) TPW (mm), c) rain rate (mm/hour), d) total cloud water (mm),
1490 and e) surface skin temperature (K). The vertical black bracket superimposed on the
1491 mean denotes the standard error of the mean. The green dashed line is the number of
1492 samples, indicated by the scale on the right.

1493

1494 Figure 6. Mean and standard of the mean for the F16- gb-GPS TPW biases varying with
1495 a) wind speed (m/s), b) TPW (mm), c) rain rate (mm/hour), d) total cloud water (mm) and
1496 e) surface skin temperature (K). The vertical black bracket superimposed on the mean
1497 denotes the standard error of the mean. The green dashed line is the number of samples,
1498 indicated by the scale on the right.

1499

1500 Figure 7. The time series of monthly mean F16 – COSMIC TPW differences under a)
1501 clear, b) cloudy, c) cloudy but non-precipitation, and d) precipitation conditions. The
1502 black line is the mean difference for microwave radiometer minus COSMIC; the vertical
1503 lines superimposed on the mean values are the standard error of the mean. The number of
1504 the monthly MW radiometer- COSMIC pairs is indicated by the green dashed line (scale
1505 on the right Y axis).

1506

1507 Figure 8. The time series of de-seasonalized TPW differences (microwave radiometer –
1508 COSMIC) under cloudy skies for a) F15, b) F16, c) F17, d) WindSat. The black line is
1509 the mean difference for microwave radiometer minus COSMIC; the vertical lines
1510 superimposed on the mean values are the standard error of the mean. The number of the
1511 monthly MW radiometer- COSMIC pairs is indicated by the green dashed line (scale on
1512 the right Y axis). The trends are shown by solid red line. The 95% confidence intervals
1513 for slopes are shown in the parentheses.

1514

1515 Figure 9. The de-seasonalized time series of monthly mean TPW for all MW, and
1516 COSMIC observations under all sky conditions. The red and blue dashed lines are the
1517 best fit of de-seasonalized COSMIC and MW TPW time series, respectively.

Deleted: global

Deleted: instruments

1518

1519 Figure 10. The global map of TPW trend in mm/decade over oceans using all F16, F17,
1520 WindSat data from 2006 to 2013.

Deleted: sa

1521

1522 Figure 11. Global mean TPW monthly anomaly (mm) relative to 1981-2010 mean for
1523 ocean regions 60°S-60°N from ERA-Interim reanalysis (green), RSS microwave (blue) and
1524 COSMIC (red). (Based on data from Mears et al., 2017).

1525

1526

1527

1528

1529

1530

1531

1532

1533

1534

1535

1536

1537

1538

1539

1540

1541

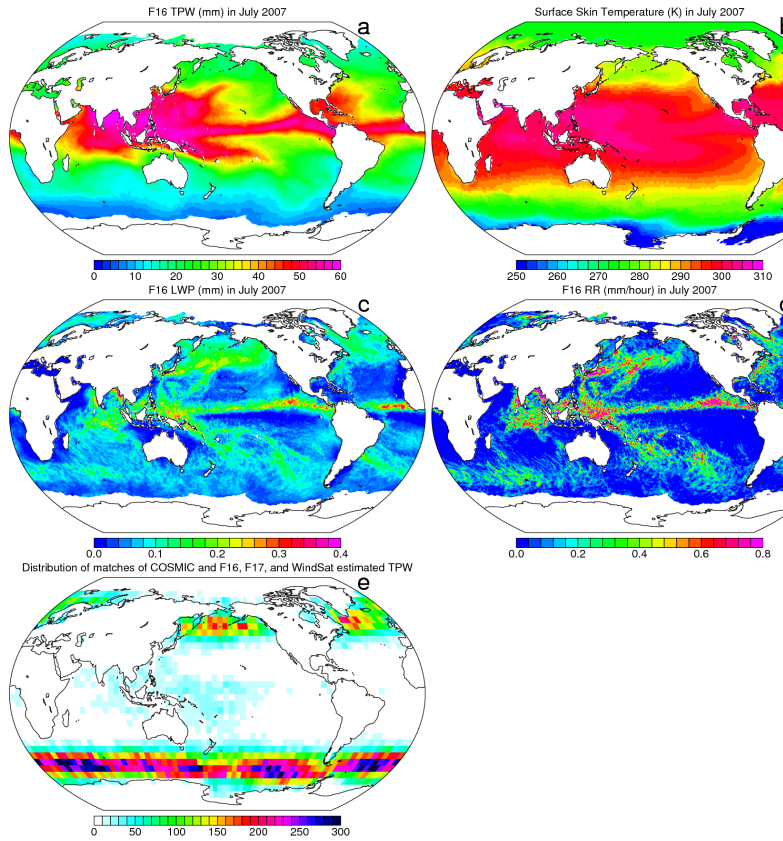
1542

1543

1544

1545

1549
1550



1551
1552
1553
1554
1555
1556
1557
1558
1559
1560
1561
1562
1563

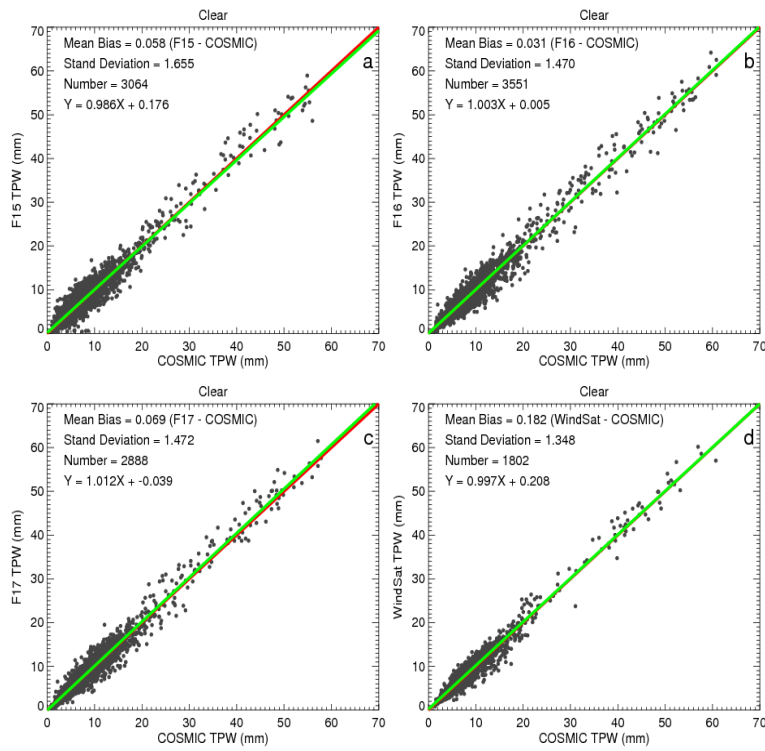
Figure 1. a-e: The RSS V7.0 monthly mean F16 SSM/I a) TPW (in mm), b) surface skin temperature (in K), c) liquid water path (LWP, in mm), d) rain rate (RR, in mm/hour), and e) distribution of matches of COSMIC RO and F16, F17 and WindSat estimations of TPW used in this study.

Deleted: . [1]

Formatted: Font:Times

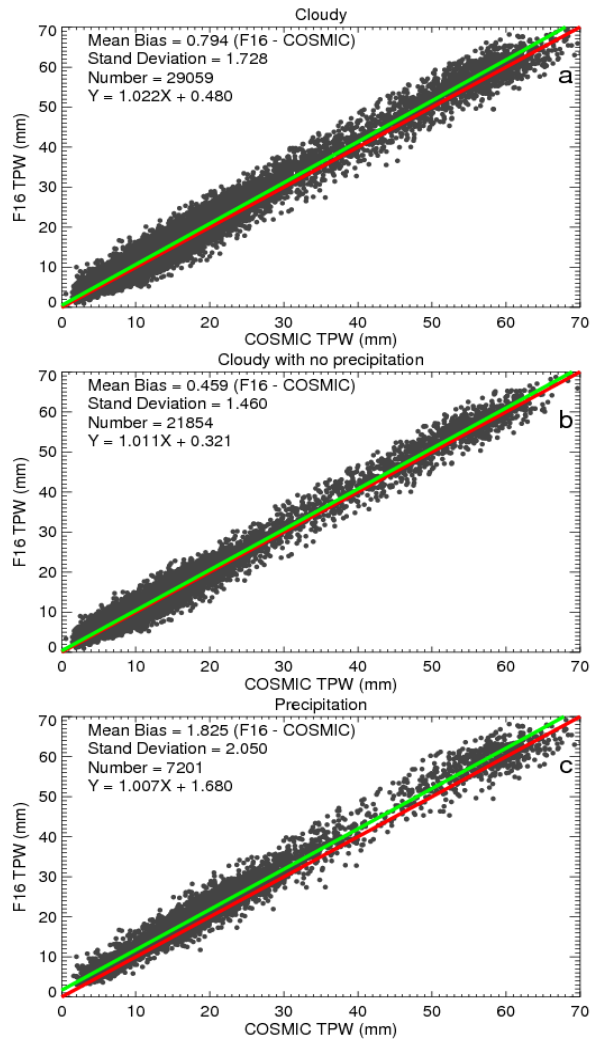
- Deleted: d
- Deleted: and
- Deleted: .
- Deleted: SSM/I (
- Deleted: SAT
- Deleted:)

1572
1573
1574



1575
1576
1577
1578
1579
1580
1581
1582
1583
1584
1585

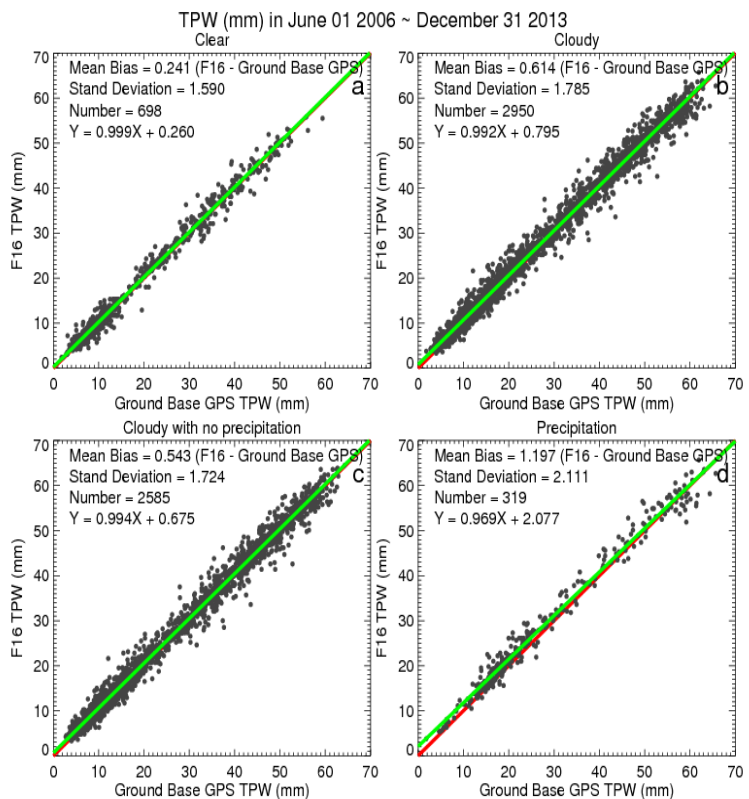
Figure 2. TPW scatter plots for the COSMIC and RSS Version 7.0 pairs under clear conditions for a) F15, b) F16, c) F17, and d) WindSat.



1586
 1587
 1588
 1589
 1590
 1591
 1592
 1593

Figure 3. TPW scatter plots for the COSMIC and RSS Version 7.0 F16 SSM/I pairs under a) cloudy, b) cloudy but non-precipitation, and c) precipitation conditions.

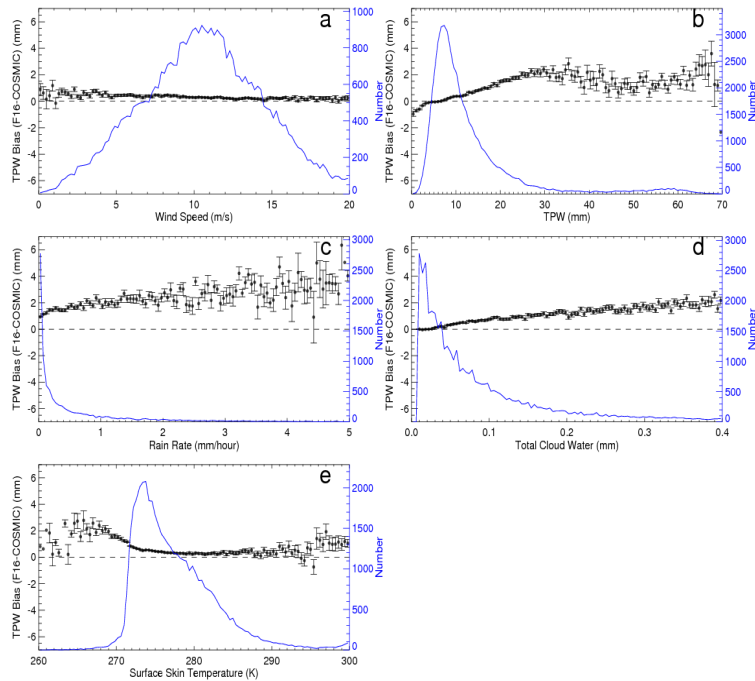
1594
1595



1596
1597
1598
1599
1600
1601
1602
1603
1604
1605
1606
1607
1608
1609
1610
1611

Figure 4. TPW scatter plots for the gb-GPS and RSS Version 7.0 F16 SSM/I pairs from June 2006 to December 2013 under a) clear, b) cloudy, c) cloudy but non-precipitation, and d) precipitation conditions.

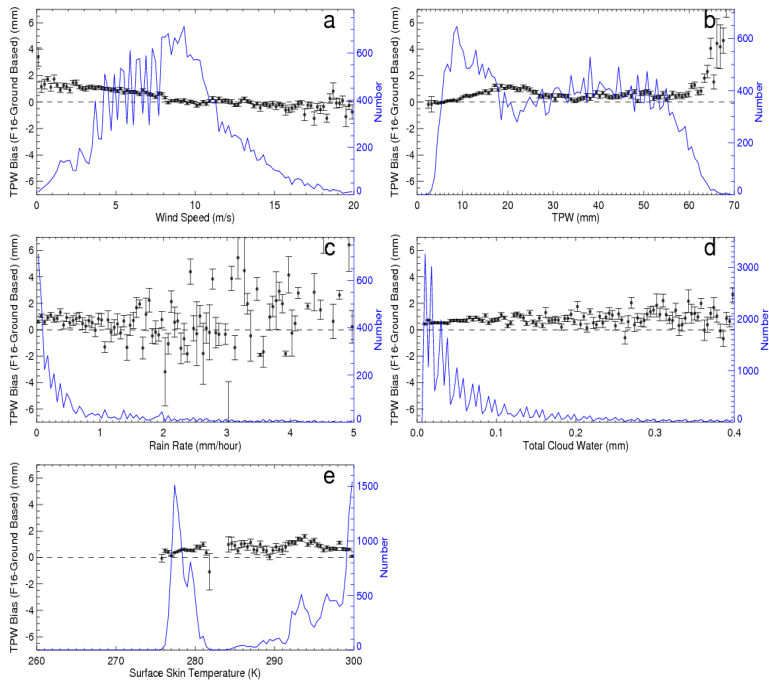
1612
1613



1614
1615
1616
1617
1618
1619
1620
1621
1622
1623
1624
1625
1626
1627
1628
1629
1630
1631
1632
1633

Figure 5. Mean and standard of the mean for the F16-COSMIC TPW biases varying with a) wind speed (m/s), b) TPW (mm), c) rain rate (mm/hour), d) total cloud water (mm), and e) surface skin temperature (K). The vertical black bracket superimposed on the mean denotes the standard error of the mean. The green dashed line is the number of samples, indicated by the scale on the right.

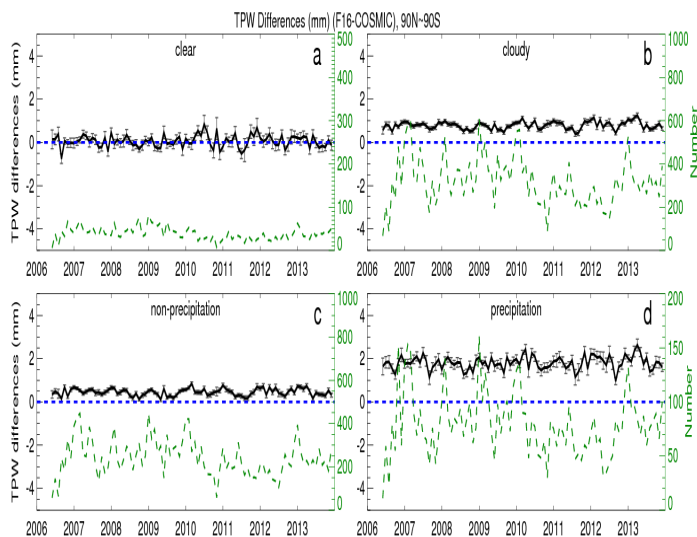
1634
1635
1636
1637
1638



1639
1640
1641
1642
1643
1644
1645
1646
1647
1648
1649
1650
1651
1652
1653
1654
1655

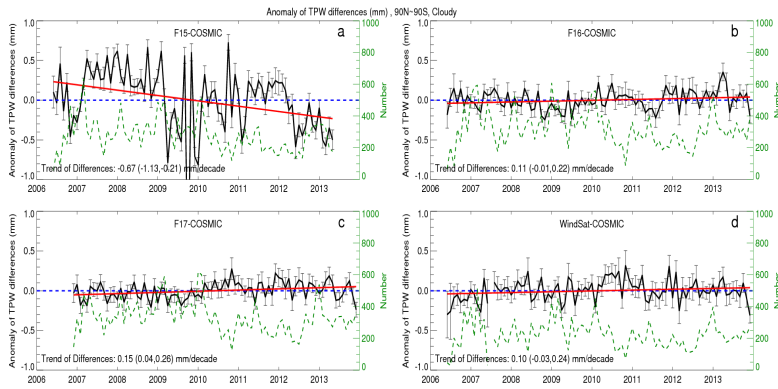
Figure 6. Mean and standard of the mean for the F16- gb-GPS TPW biases varying with a) wind speed (m/s), b) TPW (mm), c) rain rate (mm/hour), d) total cloud water (mm) and e) surface skin temperature (K). The vertical black bracket superimposed on the mean denotes the standard error of the mean. The green dashed line is the number of samples, indicated by the scale on the right.

1656
1657
1658



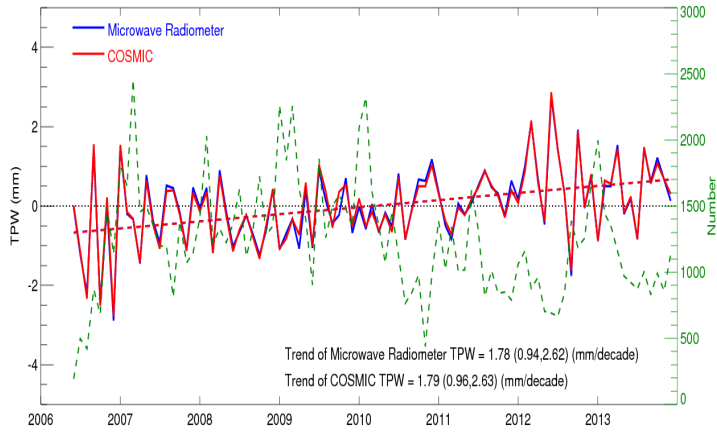
1659
1660
1661
1662
1663
1664
1665
1666
1667
1668
1669
1670
1671
1672
1673

Figure 7. The time series of monthly mean F16 – COSMIC TPW differences under a) clear, b) cloudy, c) cloudy but non-precipitation, and d) precipitation conditions. The black line is the mean difference for microwave radiometer minus COSMIC; the vertical lines superimposed on the mean values are the standard error of the mean. The number of the monthly MW radiometer- COSMIC pairs is indicated by the green dashed line (scale on the right Y axis).



1674
 1675
 1676
 1677
 1678
 1679
 1680
 1681
 1682
 1683
 1684
 1685
 1686
 1687
 1688
 1689
 1690
 1691
 1692
 1693
 1694
 1695
 1696
 1697
 1698

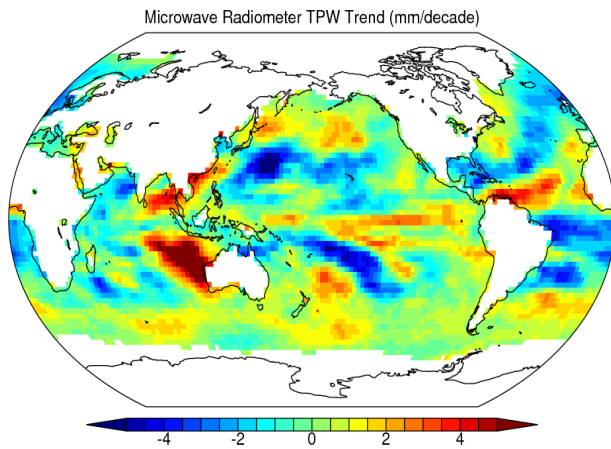
Figure 8. The time series of de-seasonalized TPW differences (microwave radiometer – COSMIC) under cloudy skies for a) F15, b) F16, c) F17, d) WindSat. The black line is the mean difference for microwave radiometer minus COSMIC; the vertical lines superimposed on the mean values are the standard error of the mean. The number of the monthly MW radiometer- COSMIC pairs is indicated by the green dashed line (scale on the right Y axis). The trends are shown by solid red line. The 95% confidence intervals for slopes are shown in the parentheses.



1699
 1700
 1701
 1702
 1703
 1704
 1705
 1706
 1707
 1708
 1709
 1710
 1711
 1712
 1713
 1714
 1715
 1716
 1717
 1718
 1719
 1720
 1721
 1722

Figure 9. The de-seasonalized time series of monthly mean TPW for all MW and COSMIC observations under all sky conditions. The red and blue dashed lines are the best fit of de-seasonalized COSMIC and MW TPW time series, respectively.

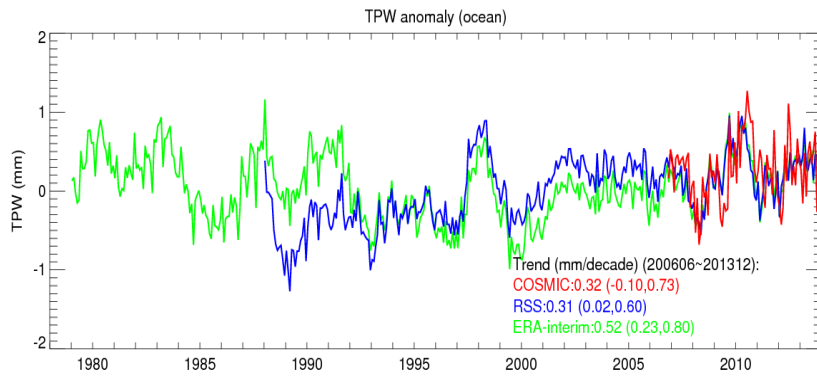
Deleted: global
Deleted: instruments



1725
 1726
 1727
 1728
 1729
 1730
 1731
 1732
 1733
 1734
 1735
 1736
 1737
 1738

Figure 10. The global map of TPW trend in mm/decade over oceans using all F16, F17, WindSat data from 2006 to 2013.

Deleted: s



Formatted: Font color: Black

1740

1741

1742 Figure 11. Global mean TPW monthly anomaly (mm) relative to 1981-2010 mean for
 1743 ocean regions 60°S-60°N from ERA-Interim reanalysis (green), RSS microwave (blue) and
 1744 COSMIC (red). (Based on data from Mears et al., 2017).

